Multiaxial fatigue assessment of welded steel details according to the peak stress method: Industrial case studies

Elsevier Editorial System(tm) for International Journal of Fatigue
Manuscript Draft

Manuscript Number:

Title: MULTIAXIAL FATIGUE ASSESSMENT OF WELDED STEEL DETAILS ACCORDING TO THE PEAK STRESS METHOD: INDUSTRIAL CASE STUDIES

Article Type: Original Research Paper

Keywords: Multiaxial fatigue; Welded joints; Local Approaches; Fatigue design; Coarse Mesh.

Corresponding Author: Professor Giovanni Meneghetti, Prof

Corresponding Author's Institution: University of Padova

First Author: Giovanni Meneghetti, Prof

Order of Authors: Giovanni Meneghetti, Prof; Alberto Campagnolo, Assistant professor; Vittorio Babini; Matteo Riboli; Andrea Spagnoli, Full Professor

Manuscript Region of Origin: Europe

UNIVERSITÀ DEGLI STUDI DI PADOVA

Prof M.N. James

School of Marine Science & Engineering, University of Plymouth, Drake Circus, Plymouth, PL4 8AA, ENGLAND

Dear Prof. James,
please find attached the manuscript entitled:

MULTIAXIAL FATIGUE ASSESSMENT OF WELDED STEEL DETAILS ACCORDING TO THE PEAK STRESS METHOD: INDUSTRIAL CASE STUDIES

Authors: Giovanni Meneghetti*, Alberto Campagnolo, Vittorio Babini, Matteo Riboli, Andrea Spagnoli

*Corresponding author: giovanni.meneghetti@unipd.it, tel. 0039 049 8276751, fax 0039 049 8276785

for possible publication in the **International Journal of Fatigue.**

The paper has not been published previously and is not under consideration for publication elsewhere

.

Yours sincerely,

Giovanni Meneghetti

Giovanni Meneghetti

Padova, January 21st 2019

Prof. Giovanni Meneghetti
Department of Industrial Engineering - University of Padova
via Venezia, 1 - 35131 Padova (Italy)
Tel. +39-049-8276751 Fax +39-049-8276785
E-mail: giovanni.meneghetti@unipd.it

MULTIAXIAL FATIGUE ASSESSMENT OF WELDED STEEL DETAILS ACCORDING TO THE PEAK STRESS METHOD: INDUSTRIAL CASE STUDIES

Giovanni Meneghetti[1*], Alberto Campagnolo[1], Vittorio Babini[2], Matteo Riboli[3,4], Andrea Spagnoli[4]

[1] Department of Industrial Engineering, University of Padova, Via Venezia, 1 – 35131 Padova (Italy)
[2] Zamperla Spa, Via Monte Grappa 15/17, 36077, Altavilla Vicentina (Italy)
[3] Limitorque Fluid Power System, Flowserve S.r.l., Via Belizzi 40/42, 29122, Piacenza (Italy)
[4] Department of Engineering and Architecture, University of Parma, Parco Area delle Scienze 181/A, 43124, Parma (Italy)

* Corresponding author: giovanni.meneghetti@unipd.it, tel. 0039 049 8276751, fax 0039 049 8276785

ABSTRACT

In fatigue design of welded joints, the Peak Stress Method (PSM) is an engineering, rapid, finite element-based tool to apply the notch stress intensity factor (NSIF) approach. The PSM presents some advantages, such as: (i) coarse meshes can be adopted, the required FE size being some orders of magnitude larger than that necessary to evaluate the NSIFs from the local stress distributions; (ii) only a single stress value is sufficient to estimate the NSIFs; (iii) 2D as well as 3D FE models can be used and (iv) the design engineer is able to determine the crack initiation point when competition between weld root and weld toe failure exists. Therefore the PSM may be a convenient design tool in the industry. In the present paper, new fatigue results have been generated by testing plate-to-tube welded steel details taken from industrial case studies under in-phase bending-torsion fatigue loadings. In particular, full-penetration joints adopted in the structure of a roundabout-type carousel and fillet-welded joints for quarter-turn scotch-yoke valve actuators have been tested. Experimental fatigue results have been analysed using the PSM, which proved to determine correctly the fatigue crack initiation location. Finally, a fairly good agreement has been obtained between the experimental results and the relevant PSM-based design curves.

Keywords. Multiaxial fatigue, Welded joints, Peak Stress Method, Strain Energy Density, Coarse Mesh.

1. INTRODUCTION

Different approaches are available in standards and recommendations [1,2] to assess the fatigue strength of steel welded joints, namely the nominal stress, the hot-spot stress, the notch stress and the Linear Elastic Fracture Mechanics (LEFM) approaches. All of them assume a linear elastic material behaviour. Essentially, the nominal stress approach is based on stress calculations according to solid mechanics, so that it does not account for any stress concentration effect. The fatigue strength assessment of a welded structure is performed by comparing the calculated nominal stress with the proper design category of the joint, which primarily depends on the considered geometry and loading condition. The hot-spot stress approach requires the stress extrapolation at the weld toe, which can be performed through numerical analyses or strain gauge measurements. This method accounts for structural stress concentration effects, so that less fatigue design curves are needed as compared to the nominal stress approach. The notch stress approach [2] is based on replacing the actual weld toe and root profiles with rounded contours having notch tip radius of 1 mm [3]. According to the LEFM approach [2], the fatigue life of welded structures can be assessed by calculating the stress intensity factor (SIF) range of a propagating crack and by integrating the Paris power law.

Concerning the fatigue strength assessment of welded structures undergoing multiaxial loading conditions, there are not approaches primarily suggested by design codes and recommendations [1,2]. Former design recommendations [4] proposed to adopt either the von Mises equivalent stress range or the principal stress coupled with the uniaxial S-N curves. On the other hand, the state-of-the-art codes and recommendations [1,2] suggest to assess the multiaxial fatigue strength by using interaction equations, which relate the normal and shear stress components to the fatigue strength under pure axial and pure torsion loading, respectively. More in detail, Eurocode 3 [1] suggests to calculate an equivalent stress range, based on the linear damage summation rule proposed by

Palmgren and Miner; IIW recommendations [2] define an equivalent stress range based on the Gough-Pollard multiaxial fatigue approach.

Several contributions of the technical literature recognized that the local approaches are the most accurate for uniaxial [3] and multiaxial [5,6] fatigue strength assessments. Among these, the criteria based on Notch Stress Intensity Factors-parameters (NSIFs) [7–11], averaged strain energy density (SED) [12,13], critical plane concepts [5,6,14–17] and the Theory of Critical Distances (TCD) [6,18–20] are worth to be mentioned. In this context, Pedersen [21] has thoroughly compared different multiaxial approaches to fatigue strength assessment of welded joints, including criteria taken from standards and recommendations as well as approaches which have been proposed in the literature more recently.

Concerning local approaches based on NSIF-parameters, the Peak Stress Method (PSM) [22–31] is a rapid and approximated, FE-based technique, which enables the analyst to speed up the calculation of the NSIFs by adopting 2D as well as 3D FE models with coarse meshes. The next section will recall the theoretical background of the PSM and the local N-SIF-based criterion, i.e. the averaged SED approach. Meanwhile, the objectives of the present work are as follows:

- to present new multiaxial fatigue test results relevant to plate-to-tube full-penetration and fillet-welded steel joints taken from industrial case studies, which exhibited weld toe and weld root failures, respectively;
- to assess the fatigue crack initiation location and the fatigue life of the tested welded details by adopting the Peak Stress Method.

2. THEORETICAL BACKGROUND

According to the NSIF approach for the fatigue assessment of welded joints, the worst case condition corresponding to the sharp V-notch configuration (tip radius $\rho = 0$) is assumed both at the weld toe and the weld root sides. A notch with opening angle equal to 135° and a pre-crack (opening angle equal to 0°) are typically assumed at the weld toe and root sides, respectively, as reported in Fig. 1 [3,7,8,11,32]. Due to these assumptions, the relevant NSIFs quantify the intensity of the local linear elastic singular stress distributions evaluated in the close neighbourhood of both the weld toe and the weld root. It has been shown in the literature [33–35], that the NSIF-parameters are appropriate local stress parameters to assess the fatigue crack nucleation at the tip of sharp V-notches, in the same way as SIFs do for crack-like U-notches [36–38]. NSIFs being local stress-based parameters, they inherently correlate the fatigue life to initiate and subsequently propagate a short crack within the material volume, where the stress field is governed by the NSIF-parameters.

As an example of the NSIF-based approach, Fig. 2 shows a typical tube-to-flange welded joint subjected to multiaxial fatigue loading and highlights the stress components relevant to mode I, II and III at the toe side (mode I, II and III stresses are also present at the root side). Dealing with mode I and II loadings, the local, linear elastic, singular stress field in the vicinity of sharp V-notches has been derived by Williams [39], while the analytical expression of the local stress field tied to mode III loading is due to Qian and Hasebe [40]. The Gross and Mendelson definitions [41] of the mode I and mode II NSIFs are reported in Eqs. (1) and (2), respectively. Similarly, Eq. (3) extends Eq. (1) and (2) and defines the mode III NSIF.

$$K_1 = \sqrt{2\pi} \cdot \lim_{r \to 0} \left[\left(\sigma_{\theta\theta} \right)_{\theta=0} \cdot r^{1-\lambda_1} \right] \tag{1}$$

$$K_2 = \sqrt{2\pi} \cdot \lim_{r \to 0} \left[\left(\tau_{r\theta} \right)_{\theta=0} \cdot r^{1-\lambda_2} \right] \tag{2}$$

$$K_3 = \sqrt{2\pi} \cdot \lim_{r \to 0} \left[\left(\tau_{\theta z} \right)_{\theta=0} \cdot r^{1-\lambda_3} \right] \tag{3}$$

where λ_1, λ_2 and λ_3 are the degrees of singularity of the local stress fields [39,40] and are functions of the notch opening angle 2α, while $\sigma_{\theta\theta}$, $\tau_{r\theta}$ and $\tau_{\theta z}$ are the local, linear elastic, singular stress components referred to the notch bisector line (i.e. evaluated at $\theta=0$). Table 1 reports the values of λ_1, λ_2 and λ_3 for $2\alpha = 0°$ and 135°, which are typical at weld root and toe sides, respectively.

2.1. The averaged Strain Energy Density (SED) approach

It has been proven [7,10] that weld toe failures under fatigue loading can be rationalised by the mode I NSIF, if the notch opening angle 2α is constant. However, when weld toe and weld root sides are both potential crack initiation locations, it is not possible to directly compare the NSIFs, since their units depend on the exponents of Eqs. (1)-(3), which in turn are functions of the notch opening angle 2α. With the aim of restoring comparability, Lazzarin et al. [12,13,42] have proposed to adopt the strain energy density averaged within a material-dependent control volume, which surrounds the weld root or the weld toe and has a circular shape of radius R_0, see Fig. 1. The averaged SED parameter can be evaluated as a function of the relevant NSIFs by taking advantage of the closed-form expression reported in Eq. (4), which assumes a general multiaxial stress state [13], i.e. a mixed mode I+II+III loading:

$$\Delta\overline{W} = \frac{e_1}{E}\left[\frac{\Delta K_1}{R_0^{1-\lambda_1}}\right]^2 + \frac{e_2}{E}\left[\frac{\Delta K_2}{R_0^{1-\lambda_2}}\right]^2 + \frac{e_3}{E}\left[\frac{\Delta K_3}{R_0^{1-\lambda_3}}\right]^2 \qquad (4)$$

In previous expression E is the Young's modulus of the material, e_1, e_2 and e_3 are parameters depending on the notch opening angle 2α and on the Poisson's ratio ν; finally ΔK_1, ΔK_2 and ΔK_3 are the ranges (maximum value minus minimum value) of the NSIF-parameters. Table 1 reports the values of e_1, e_2 and e_3 calculated for $2\alpha = 0°$ (typical at the weld root) and 135° (typical at the weld toe) assuming a Poisson's ratio $\nu = 0.3$, valid for structural steels [13]. The structural volume size

R_0 to be adopted for the fatigue strength assessment of welded joints has been calibrated in [10,12] by equalling the averaged SED in the following two situations:

- the high-cycle fatigue strength (typically at $N_A = 2 \cdot 10^6$ cycles) of butt ground welded joints;
- the high-cycle fatigue strength (again at $N_A = 2 \cdot 10^6$ cycles) of welded joints exhibiting fatigue crack initiation from the weld toe, where the opening angle is $2\alpha \approx 135°$.

In the case of arc-welded joints made of structural steels tested in the as-welded conditions, R_0 resulted equal to 0.28 mm.

It should be noted that Lazzarin and co-workers adopted Eq. (4) to correlate experimental data obtained by fatigue testing welded joints in the as-welded conditions with a load ratio R ≥ 0 [10–13]. The mean stress effect is not taken into account by Eq. (4). This approach is consistent with the standards and recommendations [1,2], where detail categories are independent of the applied mean stress for as-welded joints, at least when R ≥ -0.25 and residual stresses have medium or high tensile values, if compared to the yield strength of the base material. On the other hand, when stress-relieved joints are considered, the mean stress effect on the fatigue behaviour is fully effective and, therefore, it is considered in fatigue design [1,2]. Accordingly, for stress-relieved joints the mean stress effect is included in the averaged SED expression:

$$\Delta\overline{W} = c_{w1}\frac{e_1}{E}\left[\frac{\Delta K_1}{R_0^{1-\lambda_1}}\right]^2 + c_{w2}\frac{e_2}{E}\left[\frac{\Delta K_2}{R_0^{1-\lambda_2}}\right]^2 + c_{w3}\frac{e_3}{E}\left[\frac{\Delta K_3}{R_0^{1-\lambda_3}}\right]^2 \tag{5}$$

where the parameters c_{wi} (i = 1, 2, 3 indicates the loading mode) account for the nominal load ratio R and are defined as follows [11]:

$$c_w(R) = \begin{cases} \dfrac{1+R^2}{(1-R)^2} & \text{if} \quad -1 \le R \le 0 \\ \dfrac{1-R^2}{(1-R)^2} & \text{if} \quad 0 \le R < 1 \end{cases} \tag{6}$$

As master cases, the coefficient c_w equals 1 for R = 0 and 0.5 for $R = -1$.

The NSIF-based approach applied to industrial situations may exhibit a major drawback, in that it requires very refined FE meshes, if the definitions (1)-(3) are applied by post-processing numerical results [7]. This drawback is more pronounced when three-dimensional structures are considered, the numerical analyses being more time-consuming. To overcome this issue, the averaged SED can be evaluated by adopting coarse meshes inside the structural volume of radius R_0 according to the so-called “direct approach” Eq. (7) [43]:

$$\Delta\bar{W} = \frac{\sum_{V(R_0)} W_{FEM,i}}{V(R_0)} \tag{7}$$

In Equation (7) the strain energy $W_{FEM,i}$ is evaluated at the integration points of the i-th finite element included in the structural volume (or area in 2D problems, as shown in Fig. 1) of radius R_0. Alternatively, the Peak Stress Method may also be adopted to rapidly estimate the NSIF-parameters to be input in Eqs. (4) and (5) [22]. The main advantages of the PSM can be listed as follows: (i) it is not necessary to model the material-dependent structural volume having size R_0; (ii) coarse FE meshes can be employed, even coarser than those suggested in [43] to apply Eq. (7); (iii) only the linear elastic peak stresses evaluated at the point of stress singularity suffice to be considered; therefore the set of stress-distance data necessary to calculate the NSIFs according to definitions (1)-(3) are no-longer necessary.

2.2. The Peak Stress Method (PSM)

The PSM was inspired by the ‘crack tip stress method’ developed by Nisitani and Teranishi [44,45] to estimate the mode I SIF of a circumferential crack originating from an ellipsoidal cavity. The PSM has been justified theoretically and it has been extended to estimate the NSIF of sharp and open V-notches loaded under mode I [22,23], the SIF of cracks under mode II [24] and the NSIF of open V-notches subjected to mode III [25]. Radaj [46] has recently reviewed thoroughly the SED approach and its relationship with the PSM.

The PSM is a rapid, approximate, FE-based numerical method to calculate the NSIFs K_1, K_2 and K_3 (Eqs. (1)-(3)), starting from the linear elastic, opening ($\sigma_{\theta\theta,\theta=0,peak}$), in-plane shear ($\tau_{r\theta,\theta=0,peak}$) and out-of-plane shear ($\tau_{\theta z,\theta=0,peak}$) peak stresses, respectively, which are calculated at the V-notch tip (r = 0, θ = 0°) by FEM, according to Fig. 3. The following dimensionless ratios have been defined and calibrated in the original contributions [22,24,25]:

$$K^{*}_{FE} = \frac{K_1}{\sigma_{\theta\theta,\theta=0,peak} \cdot d^{1-\lambda_1}} \tag{8}$$

$$K^{**}_{FE} = \frac{K_2}{\tau_{r\theta,\theta=0,peak} \cdot d^{1-\lambda_2}} \tag{9}$$

$$K^{***}_{FE} = \frac{K_3}{\tau_{\theta z,\theta=0,peak} \cdot d^{1-\lambda_3}} \tag{10}$$

where *d* is the 'global element size', namely the average size of the finite elements which the FE analyst has to input before starting the free mesh generation algorithm with a commercial FE software. It is worth noting that parameters K_1, K_2 and K_3 in Eqs. (8)-(10) must be considered as the 'exact' NSIF values, i.e. obtained by applying Eqs. (1)-(3) to the results of FE analyses with very refined meshes. Examples of such 'exact' calculations are reported in the literature [7], where for a typical 10-mm-thick cruciform or T-joint the size of the smallest element in the vicinity of the point of singularity has been on the order of 10^{-5} mm.

Parameters K^{*}_{FE}, K^{**}_{FE} and K^{***}_{FE} in Eqs. (8), (9) and (10) depend on [47]: (i) element type and formulation; (ii) mesh pattern of finite elements and (iii) numerical procedure to extrapolate stresses at FE nodes. Originally, K^{*}_{FE}, K^{**}_{FE} and K^{***}_{FE} have been calibrated by adopting ANSYS® FE code and the average values of 1.38, 3.38 and 1.93, respectively, have been derived under the following conditions [22,24,25]:

- Dealing with mode I and mode II loadings (Eqs. (8) and (9)), two-dimensional, 4-node linear quadrilateral elements (PLANE 42 of ANSYS® element library or alternatively PLANE 182 with K-option 1 set to 3) must be used; dealing with mode III loading (Eq. (10)), two-dimensional, harmonic, 4-node linear quadrilateral elements (PLANE 25); three-dimensional, eight-node brick elements (SOLID 45 or alternatively SOLID 185 with K-option 2 set to 3) for all loading modes, i.e. Eqs. (8)-(10);

- the FE mesh pattern around the point of singularity must be as reported in Fig. 3 [22,24,25]: four elements must share the node at the notch tip when $2\alpha \leq 90°$ (this typically occurs at the weld root, where $2\alpha \cong 0°$), while two elements must share the node at the notch tip when $2\alpha > 90°$ (this typically occurs at the toe side, where $2\alpha \cong 135°$). It is worth noting that the PSM-standard mesh patterns reported in Fig. 3 are automatically generated by the free mesh generation algorithm of ANSYS® FE code, so that the FE analyst has only to input the 'global element size' *d*. No additional parameters or dedicated settings are required to obtain the PSM-standard mesh shown in Fig. 3. However, it should be noted that, if the mesh pattern generated by the free mesh generator is not the standard one reported in Fig. 3 (e.g. three elements are sometimes obtained at weld toe side, where $2\alpha = 135°$, instead of two), then mesh generation should be repeated by changing slightly the average element size *d* (typically up to 10%) until the standard mesh is obtained. After that, the actual *d* value has to be adopted in Eq. (8)-(10);

- Dealing with mode I and mode III loadings, Eqs. (8) and (10) can be adopted to estimate the NSIFs of V-notches having an opening angle 2α in the range from 0° to 135°; while dealing with mode II loading, Eq. (9) can be used only in the crack case ($2\alpha = 0°$);

- Concerning mode I loading (Eq. (8)), $K^{*}_{FE} = 1.38 \pm 3\%$ when the adopted mesh density ratio $a/d \geq 3$ [22]; dealing with mode II loading (Eq. (9)), $K^{**}_{FE} = 3.38 \pm 3\%$ when $a/d \geq 14$ [24]; finally, in the case of mode III loading (Eq. (10)), $K^{***}_{FE} = 1.93 \pm 3\%$ when $a/d \geq 3$ at the weld toe (i.e. $2\alpha \cong 135°$) and $a/d \geq 12$ at the root side (i.e. $2\alpha = 0°$) [25]. Concerning the mesh density ratio a/d, the reference dimension a is taken as equal to the minimum between the crack length (crack is due to the lack of penetration, i.e. l in Fig. 3), the ligament length (z in Fig. 3) and the thickness (t in Fig. 3) when the root side is analysed, while a is always the thickness (t in Fig. 3) when analysing the toe side.

These conditions of applicability for the PSM with ANSYS® FE code have been summarised in Table 2. It is worth mentioning that recent developments of the PSM include: (i) the calibration of K^{*}_{FE} and K^{**}_{FE} (Eq. (8) and (9)) by adopting six commercial FE packages [47] other than Ansys®, namely Abaqus®, Straus 7®, MSC® Patran/Nastran, Lusas®, Hypermesh/Optistruct/Hyperview® and Hypermesh/Ls-Dyna/Hyperview®; (ii) the calibration of K^{*}_{FE}, K^{**}_{FE} and K^{***}_{FE} (Eq. (8), (9) and (10)) by using 3D, ten-node, quadratic tetrahedral elements (SOLID 187 of Ansys® element library), which are particularly powerful for meshing complex 3D geometries; this recent application of the PSM proved successful to assess large-scale welded structures using High-Performance Computing [48].

To conclude, Eqs. (8)-(10) may be useful to a design engineer to rapidly estimate the NSIF-parameters K_1, K_2 and K_3 starting from the FE peak stresses $\sigma_{\theta\theta,\theta=0,peak}$, $\tau_{r\theta,\theta=0,peak}$ and $\tau_{\theta z,\theta=0,peak}$, respectively, calculated from FE analyses with coarse meshes.

2.3. The equivalent stress for fatigue design

2.3.1 *The sharp notch case (Figs 1-3)*

The averaged SED, Eqs. (4) or (5), can be expressed in closed-form as a function of the relevant NSIFs, which in turn can readily be evaluated by FEM using the PSM (Eqs. (8)-(10)). Therefore it is straightforward to estimate the averaged SED from the linear elastic peak stresses $\sigma_{\theta\theta,\theta=0,peak}$, $\tau_{r\theta,\theta=0,peak}$ and $\tau_{\theta z,\theta=0,peak}$ calculated at the point of singularity by using coarse FE meshes according to the PSM. In more detail, by substituting Eqs ((8)-(10)) into Eq. (5) and by considering an equivalent uniaxial plane strain state , for which the strain energy density is $W = \left(1-\nu^2\right)\sigma^2_{eq,peak}/2E$, then an equivalent peak stress can be defined according to Eq. (11) [30,31]:

$$\Delta\overline{W} = c_{w1}\frac{e_1}{E}\left[K^{*}_{FE}\cdot\Delta\sigma_{\theta\theta,\theta=0,peak}\cdot\left(\frac{d}{R_0}\right)^{1-\lambda_1}\right]^2 + c_{w2}\frac{e_2}{E}\left[K^{**}_{FE}\cdot\Delta\tau_{r\theta,\theta=0,peak}\cdot\left(\frac{d}{R_0}\right)^{1-\lambda_2}\right]^2 + c_{w3}\frac{e_3}{E}\left[K^{***}_{FE}\cdot\Delta\tau_{\theta z,\theta=0,peak}\cdot\left(\frac{d}{R_0}\right)^{1-\lambda_3}\right]^2 \rightarrow= \frac{1-\nu^2}{2E}\Delta\sigma^2_{eq,peak} \tag{11}$$

After re-arranging, the equivalent peak stress takes the form:

$$\Delta\sigma_{eq,peak} = \sqrt{c_{w1}\cdot f^2_{w1}\cdot\Delta\sigma^2_{\theta\theta,\theta=0,peak} + c_{w2}\cdot f^2_{w2}\cdot\Delta\tau^2_{r\theta,\theta=0,peak} + c_{w3}\cdot f^2_{w3}\cdot\Delta\tau^2_{\theta z,\theta=0,peak}} \tag{12}$$

Eq. (12) includes the coefficients f_{w1}, f_{w2} and f_{w3}, which weight the peak stresses inside the material-dependent structural volume centred at the notch tip and having size R_0, i.e. along both radial r and angular θ directions (see Fig. 2). The weighting-parameters f_{w1}, f_{w2} and f_{w3} are defined by Eqs. (13a)-(13c) [30,31], which derive from the comparison of Eqs. (11) and (12).

$$f_{w1} = K^{*}_{FE}\cdot\sqrt{\frac{2e_1}{1-\nu^2}}\cdot\left(\frac{d}{R_0}\right)^{1-\lambda_1} \tag{13a}$$

$$f_{w2} = K^{**}_{FE}\cdot\sqrt{\frac{2e_2}{1-\nu^2}}\cdot\left(\frac{d}{R_0}\right)^{1-\lambda_2} \tag{13b}$$

$$f_{w3} = K_{FE}^{***} \cdot \sqrt{\frac{2e_3}{1-\nu^2}} \cdot \left(\frac{d}{R_0}\right)^{1-\lambda_3} \tag{13c}$$

Table 1 lists the coefficients f_{w1}, f_{w2} and f_{w3} calculated from Eq. (13), by adopting a finite element size d = 1 mm, a notch opening angle 2α = 0° (typical at weld root) or 135° (typical at weld toe), respectively, and a size of the structural volume R_0 = 0.28 mm [10,12]. It is worth noting that the equivalent peak stress Eq. (12) is independent of the global element size d, even if coefficients f_{w1}, f_{w2} and f_{w3} and peak stresses are functions of d by virtue of Eq. (11).

When analysing the weld root under pure mode I loading or the weld toe, where $2\alpha > 102°$ [39,49], mode II stress components are null or non-singular, respectively, so that Eq. (12) simplifies as follows:

$$\Delta\sigma_{eq,peak} = \sqrt{c_{w1} \cdot f_{w1}^2 \cdot \Delta\sigma_{\theta\theta,\theta=0,peak}^2 + c_{w3} \cdot f_{w3}^2 \cdot \Delta\tau_{\theta z,\theta=0,peak}^2} \tag{14}$$

As discussed in Section 2.1, the fatigue behaviour of as-welded joints is not affected by the nominal load ratio R, so that the parameters c_{wi} (i = 1, 2, 3) must be set equal to 1 and Eqs. (12) and (14) can be simplified to Eqs. (15) and (16), respectively:

$$\Delta\sigma_{eq,peak} = \sqrt{f_{w1}^2 \cdot \Delta\sigma_{\theta\theta,\theta=0,peak}^2 + f_{w2}^2 \cdot \Delta\tau_{r\theta,\theta=0,peak}^2 + f_{w3}^2 \cdot \Delta\tau_{\theta z,\theta=0,peak}^2} \tag{15}$$

$$\Delta\sigma_{eq,peak} = \sqrt{f_{w1}^2 \cdot \Delta\sigma_{\theta\theta,\theta=0,peak}^2 + f_{w3}^2 \cdot \Delta\tau_{\theta z,\theta=0,peak}^2} \tag{16}$$

2.3.2 *The radiused notch case (Fig. 4)*

Previous expressions Eqs. (12), (14)-(16), are valid when the weld root and the weld toe radii $\rho \approx 0$, i.e. when stresses are singular. In the special case of a radiused weld toe ($\rho > 0$), the averaged SED, $\Delta\overline{W}$, can directly be calculated according to the 'direct approach' (Eq. (7)) inside the structural volume having the ‘crescent shape’ geometry defined in Fig. 4 as proposed by Lazzarin and Berto [50] for blunt notches. Finally, the equivalent peak stress can be calculated according to the following expression:

$$c_w \cdot \Delta\bar{W} = \frac{1-\nu^2}{2E} \cdot \Delta\sigma^2_{eq,peak} \quad \rightarrow \qquad \Delta\sigma_{eq,peak} = \sqrt{c_w \cdot \frac{2 \cdot E \cdot \Delta\bar{W}}{1-\nu^2}} \tag{17}$$

The equivalent peak stress, according to Eqs. (12), (14)-(16), has previously been adopted to summarise experimental results obtained by fatigue testing structural steel welded details under pure axial/pure bending [24,26–28], pure torsion [25,29] or multiaxial [31] loading conditions.

3. FATIGUE TESTS ON PLATE-TO-TUBE STEEL WELDED DETAILS

3.1. Specimen geometries, materials and testing conditions

Experimental fatigue results have been generated by testing plate-to-tube welded steel details under multiaxial stresses. Industrial case studies have been considered, as follows:

- full-penetration joints (see model 1 in Table 3) both in the as-welded and stress-relieved conditions, which are adopted in the structure of a roundabout-carousel;
- fillet-welded joints (see model 2 in Table 3) in the stress-relieved conditions, which are present in a quarter-turn scotch yoke for valve actuators, typically used in oil & gas, power and chemical industries.

The joint geometries are reported in Table 3, some details being confidential and then not reported in the Table; the materials and welding processes are reported in Table 4. Table 5 shows that half of the full-penetration joints (model 1 of Table 3) and all fillet-welded joints (model 2 of Table 3) were stress-relieved prior to testing.

3.2. Residual stress measurements

To evaluate the effectiveness of the stress-relieving heat treatment performed on full-penetration joints (model 1 of Table 3), residual stresses were experimentally measured by the X-ray diffraction method. Figure 5 reports the measurement path originating from the weld toe and the axial σ_{xx} and hoop σ_{zz} residual stress components, while Table 6 reports details on the adopted X-ray devices and the experimental parameters. First, two different X-ray devices, i.e. GNR SpiderX and Stresstech G3 available at the University of Padova (UNIPD) and Fraunhofer IWM-Institute, respectively, have been adopted to measure residual stresses in two different as-welded specimens, to compare residual stresses (i) in different specimens and (ii) using different X-ray devices. The measured axial σ_{xx} and hoop σ_{zz} residual stresses have been reported in Fig. 6 as a function of the distance from the weld toe. Specimen 2 was analysed both at UNIPD and at the IWM Fraunhofer. Fig. 6 shows that both the analysed specimens have high compressive residual stresses, particularly in the axial direction, as typically observed in tubular joints [51]. Fig. 6 shows a certain scatter of the residual stress field, either in different specimens analysed with the same X-ray device and in the same specimen analysed with different X-ray devices.

After that, the evolution of residual stresses during fatigue testing has been measured along the path of Fig. 5 on two specimens, one as-welded and the other stress-relieved, by adopting the GNR® SpiderX device. More precisely, residual stresses have been measured before and after fatigue testing with a load range of 162 kN for approximately one quarter and for half of the number of cycles to failure, in order to monitor the evolution of residual stresses during cyclic loading. Results have been reported in Fig. 7; by comparing as-welded and stress-relieved specimens before fatigue testing ($N/N_f = 0$), it is seen that the stress-relieving heat treatment reduced, but not completely removed, the axial residual stresses σ_{xx}; on the other hand, the hoop residual stresses σ_{zz} were still compressive and even higher than in the as-welded joint. Finally, Fig. 7 shows that cycling loading tends to increase compressive residual stresses in as-welded specimens as well as in stress-relieved specimens; but in the latter case, a decreasing followed by increasing behaviour was noted.

3.3. Experimental set-up

The experimental fatigue tests have been carried out in standard laboratory environment by adopting a MFL axial servo-hydraulic machine, having a load capacity of 250 kN and equipped with a MTS TestStar IIm digital controller. Two specimens have been tested at the same time by using a dedicated experimental arrangement in order to apply in-phase bending-torsion loadings by using the available axial testing machine:

- concerning full-penetration joints (model 1 of Table 3), a specimen having three plates, i.e. a central plate and two lateral ones (one per each side), has been connected by means of pins to a specimen with five plates, i.e. a central plate and four lateral ones (two per each side) as reported in Figs. 8a and b. The central plates of the pair of specimens being rotated by 20° with respect to the side ones, they could be connected to the upper grip and the lower grip, respectively, by means of connecting pins. As a result, the tube of each specimen was subjected to in-phase bending and torsion fatigue loadings.
- concerning fillet-welded joints (model 2 of Table 3), four keys have been adopted to connect each yoke tube to a shaft, the ends of which have been connected to steel plates (see Figs. 8c and d) by using eight keys, i.e. four for each side. Slider blocks located at a distance h from the tube axis, as sketched in model 2 of Table 3, transferred the load applied by the testing machine (F in Fig. 8c) to the yokes wings. Therefore, in-phase mode (I+III) multiaxial fatigue stresses were generated at the weld root and at the weld toe of the fillet-welds (see also [52] for more details).

The experimental fatigue tests have been performed under closed-loop load control by imposing a constant amplitude sinusoidal load cycle with a nominal load ratio R equal to 0.1 and -1 for full-penetration and fillet joints, respectively. The load frequency has been set in the range 8÷14 Hz for full-penetration joints and in the range 3÷6 Hz for fillet-welded joints, depending on the applied load level. All in all, 14 full-penetration joints and 6 fillet-welded joints have been fatigue tested as reported in Table 5.

Fatigue failure of the specimen has been defined as the number of loading cycles N_f at which the maximum displacement S_{max} (measured by the LVDT sensor connected to the MTS controller) increased by 0.5 mm, which corresponded to a stiffness drop approximately equal to 10%. Run-out was fixed at $2 \cdot 10^6$ cycles, if no failure was detected. After each fatigue test, the maximum displacement of the hydraulic actuator S_{max} has been plotted versus the number of elapsed loading cycles (see some examples in Fig. 9) and a technical crack initiation life N_i has been defined at a 0.1-mm-increase of S_{max}. Table 5 and Fig. 9 show that the ratio between technical crack initiation life N_i and total fatigue life N_f is in the range 80÷96% for the full-penetration joints, while it is more reduced and approximately equal to 50% in the case of fillet-welded joints.

The weld toe radius at the tube side of full-penetration joints has been measured from longitudinal sections of some broken specimens. A Dino-Lite digital microscope operating at a magnification 20x was used and an average value of 2 mm has been obtained (see Fig. 10 and Table 4), the minimum and the maximum values being approximately 1.50 and 2.50 mm, respectively.

3.4. Analysis of crack initiation location and propagation paths

In all full-penetration joints, irrespective of their as-welded or stress relieved condition, the fatigue crack always initiated at the maximum bending stress region at the weld toe, then propagated along the weld toe line and in some specimens also along the tube (see examples in Fig. 11).

Concerning fillet-welded joints, multiple fatigue crack initiation locations have been observed by using dye penetrant inspections, as shown in the examples of Fig. 12. Fatigue cracks initiated from the weld root, then they emerged on the surface of the weld bead with a typical 45° inclination with respect to the weld leg (see Fig. 12 c). Additional propagating fatigue cracks have been observed on the opposite side of the same yoke wing as well as of the second wing of the same specimen (see Fig. 12b).

Finally, Figs. 11 and 12 show that the adopted “0.5-mm-displacement” failure criterion led to propagated crack lengths of several tens of a millimetre along the weld toe or the weld bead surface for full-penetration and fillet-welded joints, respectively.

3.5. Fatigue test results

Figures 13a and 13b report the number of cycles versus the applied load range ΔF (defined as maximum value minus minimum value). For each tested specimen, the figures report the number of cycles to technical crack initiation (N_i) and the number of cycles to failure (N_f) by means of open and filled markers, respectively. The scatter bands are referred to survival probabilities of 2.3 and 97.7% and are fitted over the relevant technical crack initiation data.

Figure 13a shows that full-penetration joints have an endurable force range of 74 kN, referred to a survival probability of 50% and to 2 million loading cycles, an inverse slope k equal to 3.99 and a scatter index T_F equal to 2.17. It is interesting to note that as-welded specimens exhibited longer fatigue lives than stress-relieved ones under the same load level. This behaviour was explained by the high compressive axial residual stresses especially in as-welded joints (see in comparison Figs. 7a and c), which tended to close the crack and then to retard crack propagation. At low load level as-welded and stress-relieved joints exhibited almost the same fatigue life for the same applied load. A similar behaviour was found by Yung and Lawrence [51], who tested tube-to-flange welded joints under combined bending and torsion loading and noted that fatigue strength was decreased after performing the post-welding stress-relieving heat treatment.

On the other hand, according to Fig. 13b, fillet-welded joints presented an endurable force range of 108 kN, referred to a survival probability of 50% and to 2 million loading cycles, an inverse slope k of 5.28 and a reduced scatter index, T_F being equal to 1.12.

4. FATIGUE STRENGTH ASSESSMENTS ACCORDING TO THE PSM

Given the complexity of the considered joint geometries, 3D FE models were run to convert the original experimental results from the load range applied by the testing machine to the range of the equivalent peak stress according to the PSM [23,27,31]. Table 3 shows the joint geometries and the details of the FE analyses according to the conditions of applicability of the PSM recalled in previous Sections. In particular, first the entire joint geometry has been analysed by adopting a *main model*; then, a *submodel* of the critical region , i.e. the weld toe or the weld root, has been analysed by means of the submodelling technique available in Ansys® FE code. The *main model* has been free-meshed by adopting quadratic, 10-node tetrahedral elements (SOLID 187 of the Ansys® library). Then, the *submodel* has been defined by cutting the *main model* at a distance from the weld toe (or the weld root) equal to one tube thickness. Finally, to generate the 3D mesh pattern of the *submodel*, the following procedure has been adopted:

- a 2D FE mesh of linear, quadrilateral 4-node elements (PLANE 182) having global size d has been defined to obtain the standard 2D mesh pattern of the PSM (Fig. 3);
- subsequently, the 2D mesh has been extruded about the tube axis of each joint geometry, by setting an extrusion step size equal to the average element size d and by adopting 3D 8-node brick elements (SOLID185 with K-option 2 set to 3).

The following Sections report details concerning the FE analysis of each joint geometry.

4.1 Full-penetration tube-plate joints (model 1 of Table 3)

Taking advantage of the YZ symmetry plane, the *main model* consisted of only half of the specimen and it was meshed using an average element size of 6 mm. To properly simulate the experimental configuration, the inner surface of the hole in the side plate has been constrained in the Y and Z directions, while the load range, ΔF, has been applied to the inner surface of the hole in the central plate, as shown in Table 3. The *main model* shown in Table 3 has been validated successfully by comparing the FE results with those obtained from a -45°/0°/45° strain gauge rosette fixed on the tube between the central and the side plates (see Table 3). As an example, by applying a reference load F = 180 kN, the experimental strains resulted 1175/1140/-381 $\mu\varepsilon$ and in fairly good agreement with the numerical strains at the same position, which resulted 1040/1093/-405 $\mu\varepsilon$.

To apply the PSM, a *submodel* of the weld toe region has been generated. Mode II stresses being not singular at the weld toe (since the opening angle $2\alpha = 135°$ is greater than 102° [39]), the mesh density ratio must be $a/d \geq 3$ to satisfy the conditions of applicability of the PSM at the weld toe under mode I and mode III loadings. The tube thickness being a = 8 mm, then the average element size d has been set to 8/3 = 2.66 mm. After solving the *submodel*, the peak stresses $\sigma_{\theta\theta,\theta=0,peak}$ and $\tau_{\theta z,\theta=0,peak}$ have been calculated along the weld toe line and have been reported in Fig. 14 as a function of the angular coordinate ϕ; then, the equivalent peak stress range has been evaluated from Eqs. (14) and (16) for as-welded and stress-relieved specimens, respectively. Coefficients f_{w1} and f_{w3} have been calculated from Eq. (13a) and (13c), respectively; parameters $c_{w1} = c_{w3} = 1.22$ have been adopted for stress-relieved specimens (Eq. (6) with R = 0.1). In the case of as-welded joints, it is worth noting that adopting Eq. (16) results on the safe side, because Figs. 6 and 7 have highlighted that residual stresses are highly compressive and not highly tensile, as assumed by Eq. (16).

Figure 14 reports the obtained results and shows that two potential fatigue crack initiation locations exist along the weld toe profile:

- point B (ϕ = 180°), where the absolute maximum value of the equivalent peak stress was found, but the mode I peak stress $\sigma_{\theta\theta,\theta=0,peak}$ is compressive;
- point A (ϕ = 0°), where a local maximum value of the equivalent peak stress occurs, which is 10% lower than point B, but the mode I peak stress $\sigma_{\theta\theta,\theta=0,peak}$ is tensile at point A, therefore it tends to open the initiated crack rather than close it. As a consequence, it is reasonable to anticipate the crack initiation point at point A, according to the experimental outcome documented in Fig. 11.

The model 1 reported in Table 3 has been analysed by means of the PSM by assuming a sharp V-notch at the weld toe as the worst case hypothesis; however previous Fig. 10 has highlighted that the average weld toe radius was approximately 2 mm. Therefore, an additional *main model* with weld toe radius of 2 mm has been defined by adopting again a free mesh of 10-node quadratic, tetrahedral elements with a global element size of 6 mm, which has been refined locally down to 0.07 mm, as shown in Table 3. The applied boundary conditions have been the same described previously for the sharp V-notch *main model*. The SED averaged inside the structural volume having size R_0 = 0.28 mm, $\Delta\overline{W}$, has been calculated according to the 'direct approach' (Eq. (7) and Fig. 4). Having $\Delta\overline{W}$, the equivalent peak stress has been calculated according to Eq. (17) and the results are reported again in Fig. 14. It is seen that the equivalent peak stress is approximately 10% lower as compared to the sharp V-notch model and the fatigue crack initiation location is still predicted at point A (ϕ = 0°).

4.2 Fillet-welded scotch yoke joints (model 2 of Table 3)

Taking advantage of the YZ symmetry plane, only half of the specimen geometry has been modelled in the *main model* and an average FE size of 3 mm has been adopted. To properly simulate the stress state due to the load cycle between +F and –F (Fig. 8c), two different loading conditions were run, as reported in Table 3. More precisely, a -F/2 load has been applied at the buttonhole of the yoke wing in *main model-a*, while a +F/2 force has been applied in *main model-b*. In fact, during each fatigue load cycle, the load is applied on one flank of the buttonhole during the positive half cycle, while it is applied on the opposite side of the buttonhole during the subsequent negative half cycle. The constraints are applied to the specimen by the keys and by the shaft, which in turn was restrained by the side plates; therefore, null radial displacements have been imposed to the inner surface of the tube and null hoop displacements have been imposed to the active flanks of the keyways. The constrained surfaces have properly been selected depending on the load direction, as shown in Table 3 (see in comparison *main models-a* and *-b*). The *main models* shown in Table 3 have been validated by performing strain measurements with a -45°/0°/45° strain gauge rosette fixed on the yoke wing. By applying a reference load F = -100 kN, the experimental principal strains resulted equal to 209/-292 με, while the corresponding numerical principal strains resulted equal to 245/-235 με.

The relevant *submodels* included all potential critical regions of the joint, i.e. the weld root, the weld toe at the wing side (wing-toe) and the weld toe at the tube side (tube-toe), as highlighted in Table 3. To establish the global element size to adopt, the most demanding condition to apply the PSM is dictated by the mode II loading at the weld root side: according to Table 2, the mesh density ratio must be $a/d \geq 14$, being a = 5 mm the weld leg length. Therefore, the adopted average element size d has been equal to 5/14 ≅ 0.30 mm. The peak stresses $\sigma_{\theta\theta,\theta=0,peak}$, $\tau_{r\theta,\theta=0,peak}$ and $\tau_{\theta z,\theta=0,peak}$ have been calculated from both *submodels* along the root, wing-toe and tube-toe lines. Figure 15 reports the results by using the angular coordinate ϕ and shows that mode II stresses at the weld root are small; therefore they will be disregarded in the following analysis.

Moreover, Fig. 15 shows that the peak stresses do not follow the load ratio R=-1 of the applied external force (see Table 3); then, local stress ratios $R_{\theta\theta}$ and $R_{\theta z}$ have been defined at a given angular position ϕ as the ratio between the relevant peak stresses when the external load is –F and +F, respectively:

$$R_{\theta\theta} = \frac{\left(\sigma_{\theta\theta,peak}\right)_{-F}}{\left(\sigma_{\theta\theta,peak}\right)_{+F}} \tag{18a}$$

$$R_{\theta z} = \frac{\left(\tau_{\theta z,peak}\right)_{-F}}{\left(\tau_{\theta z,peak}\right)_{+F}} \tag{18b}$$

Results are reported in Figs. 16a-c for the root, the tube-toe and the wing-toe lines, respectively. It is seen that close to the position ϕ = 0°, the stress ratio $R_{\theta\theta}$ is greater than zero; in such circumstance the stress ratio defined by Eq. (18a) is not the fatigue stress ratio, because when the load applied by the testing machine becomes zero, all stress components must also equal zero. Therefore, Fig. 16d shows that, for each completely reversed cycle of the external load, the actual stress cycle of $\sigma_{\theta\theta,peak}$ is characterised by two pulsating cycles with different stress range: one from zero to $(\sigma_{\theta\theta,peak})_{+F}$, while the second one from zero to $(\sigma_{\theta\theta,peak})_{-F}$. Therefore, the local fatigue stress ratio of the mode I peak stress $\sigma_{\theta\theta,peak}$, $R_{f,\theta\theta}$, can be defined by Eq. (19a):

$$R_{f,\theta\theta} = \begin{cases} R_{\theta\theta} & \text{if} \quad R_{\theta\theta} \le 0 \\ 0 & \text{if} \quad R_{\theta\theta} > 0 \end{cases} \tag{19a}$$

Concerning the local fatigue stress ratio of the mode III peak stress $\tau_{\theta z,peak}$, since Fig. 16a-c shows that $R_{\theta z} < 0$, then we have:

$$R_{f,\theta z} = R_{\theta z} \tag{19b}$$

Dealing with the equivalent peak stress calculation in the case of local stress ratio $R_{\theta\theta} > 0$, the actual two-levels stress cycle $\sigma_{\theta\theta,peak}$ (see Fig. 16d) has been treated by applying the linear damage summation according to Palmgren and Miner. The equivalent peak stress for each pulsating cycle, i.e. $\left(\Delta\sigma_{eq,peak}\right)_{+F,\sigma_{\theta\theta}}$ and $\left(\Delta\sigma_{eq,peak}\right)_{-F,\sigma_{\theta\theta}}$, has first been defined:

$$\begin{cases} \left(\Delta\sigma_{eq,peak}\right)_{+F,\sigma_{\theta\theta}} = f_{w1} \cdot \left[\left(\sigma_{\theta\theta,peak}\right)_{+F}\right] & \text{if} \quad R_{\theta\theta} > 0 \\ \left(\Delta\sigma_{eq,peak}\right)_{-F,\sigma_{\theta\theta}} = f_{w1} \cdot \left[\left(\sigma_{\theta\theta,peak}\right)_{-F}\right] & \end{cases} \tag{20}$$

and subsequently the constant-amplitude, equally damaging stress has been calculated by referring to the PSM-based design curve with inverse slope k = 3 reported in [26]. Accordingly, the constant-amplitude equivalent peak stress referred to the mode I contribution, i.e. $\left(\Delta\sigma_{eq,peak}\right)_{\sigma_{\theta\theta}}$, has been defined as follows.

$$D = \frac{1}{\frac{\left(\Delta\sigma_{eq,peak,N_A}\right)^k \cdot N_A}{\left(\Delta\sigma_{eq,peak}\right)^k_{+F,\sigma_{\theta\theta}}}} + \frac{1}{\frac{\left(\Delta\sigma_{eq,peak,N_A}\right)^k \cdot N_A}{\left(\Delta\sigma_{eq,peak}\right)^k_{-F,\sigma_{\theta\theta}}}} = \frac{1}{\frac{\left(\Delta\sigma_{eq,peak,N_A}\right)^k \cdot N_A}{\left(\Delta\sigma_{eq,peak}\right)^k_{\sigma_{\theta\theta}}}} \tag{21}$$

$$\rightarrow \left(\Delta\sigma_{eq,peak}\right)_{\sigma_{\theta\theta}} = \left[\left(\Delta\sigma_{eq,peak}\right)^k_{+F,\sigma_{\theta\theta}} + \left(\Delta\sigma_{eq,peak}\right)^k_{-F,\sigma_{\theta\theta}}\right]^{\frac{1}{k}}$$

Finally, the equivalent peak stress, which takes into account the contributions of both mode I and mode III peak stresses, has been calculated as follows:

$$\Delta\sigma_{eq,peak} = \begin{cases} \sqrt{c_{w1} \cdot f_{w1}^2 \cdot \left[\left(\sigma_{\theta\theta,peak}\right)_{+F} - \left(\sigma_{\theta\theta,peak}\right)_{-F}\right]^2 + c_{w3} \cdot f_{w3}^2 \cdot \Delta\tau^2_{\theta z,\theta=0,peak}} & \text{if} \quad R_{\theta\theta} \leq 0 \\ \sqrt{\left[\left(\Delta\sigma_{eq,peak}\right)^k_{+F,\sigma_{\theta\theta}} + \left(\Delta\sigma_{eq,peak}\right)^k_{-F,\sigma_{\theta\theta}}\right]^{\frac{2}{k}} + c_{w3} \cdot f_{w3}^2 \cdot \Delta\tau^2_{\theta z,\theta=0,peak}} & \text{if} \quad R_{\theta\theta} > 0 \end{cases} \tag{22}$$

where coefficients c_{w1} and c_{w3} have been introduced because all fillet-welded joints having been tested under stress-relieved conditions and have been calculated from Eq. (6) by substituting the local fatigue stress ratios $R_{f,\theta\theta}$ (Eq. (19a)) and $R_{f,\theta z}$ (Eq. (19b)), respectively.

Figure 17 reports the results obtained by applying Eq. (22) along the root, the wing-toe and the tube-toe lines, and shows that the absolute maximum of the equivalent peak stress occurs along the weld root line at an angle ϕ of about 5°. According to the experimental evidences reported in Fig. 12, it can be concluded that the PSM allows a proper estimation of the fatigue crack initiation location also in the fillet-welded joints.

5. ASSESSMENT OF WELD TOE AND WELD ROOT FATIGUE FAILURES

After applying the PSM, the experimental results have been converted from the applied load range (see Fig. 13) to the range of equivalent peak stress calculated at the point of crack initiation. In order to select the appropriate PSM-based design curve, it has been recently argued that the contribution of shear as compared to normal stresses must first be quantified. To this aim, a local biaxiality ratio has been defined recently as the ratio between the energy contributions tied to the shear modes of loading, i.e. mode II and III, and the energy contribution tied to the opening mode, i.e. mode I [53–55]. This ratio can be expressed as a function of the peak stresses $\tau_{r\theta,\theta=0,peak}$, $\tau_{\theta z,\theta=0,peak}$ and $\sigma_{\theta\theta,\theta=0,peak}$, respectively, according to Eq. (23):

$$\lambda_{local} = \frac{f_{w2}^2 \cdot \Delta\tau_{r\theta,\theta=0,peak}^2 + f_{w3}^2 \cdot \Delta\tau_{\theta z,\theta=0,peak}^2}{f_{w1}^2 \cdot \Delta\sigma_{\theta\theta,\theta=0,peak}^2} \tag{23}$$

After having re-analysed more than 400 experimental fatigue results taken from the literature and relevant to laser steel welded joints tested under uniaxial and multiaxial loading conditions [54], it was shown that fatigue results having $\lambda_{local} \lesssim 0.5$ are in agreement with the PSM-based design scatter band calibrated under prevailing mode I loading, while fatigue results having $\lambda_{local} \gtrsim 0.5$ fall inside the PSM-based design scatter band calibrated under prevailing mode III loading.

Concerning full-penetration joints, the local biaxiality ratio λ_{local} calculated at the fatigue crack initiation location, i.e. $\phi = 0$ at weld toe, is rather small and equal to λ_{local}=0.40, according to the results reported in Fig. 14. Therefore, Fig. 18 compares the experimental results with the PSM-based design scatter band previously calibrated [26] on experimental fatigue data relevant to steel welded joints tested under pure mode I loading (inverse slope of the design curve k=3). More precisely, Fig. 18 reports the experimental results evaluated according to both Eq. (14) (see Fig. 18a), i.e. by adopting the worst case hypothesis of sharp V-notch ($\rho = 0$) at weld toe, and Eq. (17) (see Fig. 18b), i.e. by adopting the radiused notch ($\rho = 2$ mm) at weld toe. Fig. 18a shows that the design scatter band is slightly on the safe side especially in the high-cycle-fatigue regime, even when technical crack initiation life is considered. On the other hand, Fig. 18b shows that the agreement between experimental results and the same design scatter band improves when considering the actual toe radius in the FE model: here only a couple of experimental data fall outside the scatter band in the high-cycle-fatigue regime.

Since full-penetration joints have λ_{local} = 0.40, which is close to the critical value 0.50 mentioned above [54], Fig. 18 includes also the PSM-based design scatter band calibrated elsewhere on experimental fatigue data relevant to steel welded joints tested under pure mode III loading [25] (inverse slope of the design curve k=5). It is observed that the experimental results are in very good agreement with this design scatter band, when considering both the sharp V-notch (ρ = 0) (Fig. 18a) and the radiused notch (ρ = 2 mm) (Fig. 18b) at weld toe. This result suggests that the limiting value of λ_{local} to distinguish between prevailing opening or shear modes of loading deserve to be investigated in more detail.

Dealing with fillet-welded joints, results reported in Figs. 15 and 17 show that the local biaxiality ratio λ_{local} equals 11.4 at the fatigue crack initiation point, which is located at an angle $\phi \approx 5°$ of the weld root. The value 11.4 being much higher than the critical value $\lambda_{local} \cong 0.50$ [54], the contribution due to mode III is predominant and then the experimental results have been compared with the PSM-based design scatter band previously calibrated on experimental fatigue data relevant to steel welded joints tested under pure mode III loading [25] (k=5). Fig. 19 shows that the experimental results expressed in terms of technical crack initiation life fall inside the PSM-based scatter band, which on the other hand exhibits a certain degree of conservatism. It is the authors' opinion that the longer experimental fatigue lives than estimated by the PSM illustrated in Fig.19 might be explained because the adopted "0.1-mm-displacement" criterion for technical crack initiation may have led to fatigue cracks propagated well beyond the material volume dominated by the singular stress distributions, which the SED criterion is actually based on. Concerning this issue, more accurate experimental techniques for damage detection are desirable in the future.

6. CONCLUSIONS

The Peak Stress Method (PSM) has been applied to analyse weld toe as well as weld root fatigue failures in plate-to-tube welded details in structural steel subjected to in-phase multiaxial stresses. The analysed industrial case studies involved (i) full-penetration joints adopted in a roundabout-type carousel tested in the as-welded as well as stress-relieved conditions and (ii) fillet-welded joints adopted in quarter-turn scotch-yoke valve actuators tested under stress-relieved conditions. Essentially, the PSM represents a rapid FE-based application of the NSIF approach, which assumes that the weld toe is a sharp V-notch having zero notch-tip radius and the weld root is a pre-crack. The design stress (i.e. the equivalent peak stress) is calculated starting from the singular, linear elastic, opening/sliding/tearing peak stresses calculated either at the weld toe or at the weld root by adopting automatically generated coarse FE mesh patterns. Physically, the equivalent peak stress expresses the strain energy density averaged within a structural volume surrounding the crack initiation point (the SED criterion).

The local stress analysis according to the PSM revealed that full-penetration joints were subjected to prevailing opening (mode I) stresses. Therefore, the experimental results relevant to full-penetration joints have been compared with the PSM-based design curve, which had been calibrated previously for pure mode I loading (inverse slope k=3). As a result, it has been observed that the scatter band is slightly on the safe side, particularly in the high-cycle-fatigue regime. If the actual 2-mm-weld toe radius is considered, the experimental results are in better agreement with the theoretical estimations. Concerning fillet-welded joints, the resulting equivalent peak stress estimated the fatigue crack initiation location according to the experimental outcome. The local stress analysis according to the PSM demonstrated prevailing shear (mode II + III) stresses. Therefore, the experimental results have been compared with the PSM-based design scatter band, which had been calibrated previously for pure mode III loading (inverse slope k=5); the experimental results were seen to fall inside the design scatter band and on the safe side. The reason for that might be explained because the adopted “0.1-mm-displacement” criterion for technical crack initiation may have led to fatigue cracks propagated well beyond the material volume dominated by the singular stress distributions, which the SED criterion is actually based on.

Because of the simplicity of a point-like method combined with the robustness of the NSIF approach, the PSM might be useful to design engineers engaged in fatigue assessments of welded joints.

ACKNOWLEDGEMENTS

Prof. Manuele Dabalà and Dr. Claudio Gennari are gratefully acknowledged for the residual stress measurements at Unipd.

REFERENCES

[1] Eurocode 3: Design of steel structures – part 1–9: Fatigue. CEN; 2005.

[2] Hobbacher AF. Recommendations for Fatigue Design of Welded Joints and Components. IIW Collection. Springer International Publishing; 2016.

[3] Radaj D, Sonsino CM, Fricke W. Fatigue Assessment of Welded Joints by Local Approaches. 2nd ed. Cambridge: Woodhead Publishing; 2006.

[4] Maddox SJ, Razmjoo GR. Interim fatigue design recommendations for fillet welded joints under complex loading. Fatigue Fract Eng Mater Struct 2001;24:329–37.

[5] Sonsino C. Multiaxial fatigue of welded joints under in-phase and out-of-phase local strains and stresses. Int J Fatigue 1995;17:55–70.

[6] Susmel L. Multiaxial notch fatigue. Cambridge, UK: Woodhead Publishing; 2009.

[7] Lazzarin P, Tovo R. A notch intensity factor approach to the stress analysis of welds. Fatigue Fract Eng Mater Struct 1998;21:1089–103.

[8] Lazzarin P, Livieri P. Notch stress intensity factors and fatigue strength of aluminium and steel welded joints. Int J Fatigue 2001;23:225–32.

[9] Atzori B, Meneghetti G. Fatigue strength of fillet welded structural steels: finite elements, strain gauges and reality. Int J Fatigue 2001;23:713–21.

[10] Lazzarin P, Lassen T, Livieri P. A notch stress intensity approach applied to fatigue life predictions of welded joints with different local toe geometry. Fatigue Fract Eng Mater Struct 2003;26:49–58.

[11] Lazzarin P, Sonsino CM, Zambardi R. A notch stress intensity approach to assess the multiaxial fatigue strength of welded tube-to-flange joints subjected to combined loadings. Fatigue Fract Eng Mater Struct 2004;27:127–40.

[12] Livieri P, Lazzarin P. Fatigue strength of steel and aluminium welded joints based on generalised stress intensity factors and local strain energy values. Int J Fract 2005;133:247–76.

[13] Lazzarin P, Livieri P, Berto F, Zappalorto M. Local strain energy density and fatigue strength of welded joints under uniaxial and multiaxial loading. Eng Fract Mech 2008;75:1875–89.

[14] Carpinteri A, Spagnoli A, Vantadori S. Multiaxial fatigue life estimation in welded joints using the critical plane approach. Int J Fatigue 2009;31:188–96.

[15] Susmel L. Three different ways of using the Modified Wöhler Curve Method to perform the multiaxial fatigue assessment of steel and aluminium welded joints. Eng Fail Anal

2009;16:1074–89.

[16] Susmel L. Four stress analysis strategies to use the Modified Wöhler Curve Method to perform the fatigue assessment of weldments subjected to constant and variable amplitude multiaxial fatigue loading. Int J Fatigue 2014;67:38–54.

[17] Susmel L, Sonsino CM, Tovo R. Accuracy of the Modified Wöhler Curve Method applied along with the rref=1mm concept in estimating lifetime of welded joints subjected to multiaxial fatigue loading. Int J Fatigue 2011;33:1075–91.

[18] Taylor D, Barrett N, Lucano G. Some new methods for predicting fatigue in welded joints. Int J Fatigue 2002;24:509–18.

[19] Susmel L. Modified Wöhler curve method, theory of critical distances and Eurocode 3: A novel engineering procedure to predict the lifetime of steel welded joints subjected to both uniaxial and multiaxial fatigue loading. Int J Fatigue 2008;30:888–907.

[20] Susmel L, Askes H. Modified Wöhler Curve Method and multiaxial fatigue assessment of thin welded joints 2012;43:30–42.

[21] Pedersen MM. Multiaxial fatigue assessment of welded joints using the notch stress approach. Int J Fatigue 2016;83:269–79.

[22] Meneghetti G, Lazzarin P. Significance of the elastic peak stress evaluated by FE analyses at the point of singularity of sharp V-notched components. Fatigue Fract Eng Mater Struct 2007;30:95–106.

[23] Meneghetti G, Guzzella C. The peak stress method to estimate the mode I notch stress intensity factor in welded joints using three-dimensional finite element models. Eng Fract Mech 2014;115:154–71.

[24] Meneghetti G. The use of peak stresses for fatigue strength assessments of welded lap joints and cover plates with toe and root failures. Eng Fract Mech 2012;89:40–51.

[25] Meneghetti G. The peak stress method for fatigue strength assessment of tube-to-flange welded joints under torsion loading. Weld World 2013;57:265–75.

[26] Meneghetti G, Lazzarin P. The Peak Stress Method for Fatigue Strength Assessment of welded joints with weld toe or weld root failures. Weld World 2011;55:22–9.

[27] Meneghetti G, Guzzella C, Atzori B. The peak stress method combined with 3D finite element models for fatigue assessment of toe and root cracking in steel welded joints subjected to axial or bending loading. Fatigue Fract Eng Mater Struct 2014;37:722–39.

[28] Meneghetti G, Campagnolo A, Berto F. Fatigue strength assessment of partial and full-penetration steel and aluminium butt-welded joints according to the peak stress method. Fatigue Fract Eng Mater Struct 2015;38:1419–31.

[29] Meneghetti G, De Marchi A, Campagnolo A. Assessment of root failures in tube-to-flange steel welded joints under torsional loading according to the Peak Stress Method. Theor Appl Fract Mech 2016;83:19–30.

[30] Meneghetti G, Campagnolo A, Rigon D. Multiaxial fatigue strength assessment of welded joints using the Peak Stress Method – Part I: Approach and application to aluminium joints. Int J Fatigue 2017;101:328–42.

[31] Meneghetti G, Campagnolo A, Rigon D. Multiaxial fatigue strength assessment of welded joints using the Peak Stress Method – Part II: Application to structural steel joints. Int J Fatigue 2017;101:343–62.

[32] Radaj D. State-of-the-art review on extended stress intensity factor concepts. Fatigue Fract Eng Mater Struct 2014;37:1–28.

[33] Boukharouba T, Tamine T, Niu L, Chehimi C, Pluvinage G. The use of notch stress intensity factor as a fatigue crack initiation parameter. Eng Fract Mech 1995;52:503–12.

[34] Verreman Y, Nie B. Early development of fatigue cracking at manual fillet welds. Fatigue Fract Eng Mater Struct 1996;19:669–81.

[35] Radaj D, Vormwald M. Advanced Methods of Fatigue Assessment. Berlin, Heidelberg: Springer Berlin Heidelberg; 2013.

[36] Smith RA, Miller KJ. Prediction of fatigue regimes in notched components. Int J Mech Sci 1978;20:201–6.
[37] Taylor D. Geometrical effects in fatigue: a unifying theoretical model. Int J Fatigue 1999;21:413–20.
[38] Atzori B, Lazzarin P, Meneghetti G. Fracture mechanics and notch sensitivity. Fatigue Fract Eng Mater Struct 2003;26:257–67.
[39] Williams ML. Stress singularities resulting from various boundary conditions in angular corners of plates in tension. J Appl Mech 1952;19:526–8.
[40] Qian J, Hasebe N. Property of eigenvalues and eigenfunctions for an interface V-notch in antiplane elasticity. Eng Fract Mech 1997;56:729–34. .
[41] Gross B, Mendelson A. Plane elastostatic analysis of V-notched plates. Int J Fract Mech 1972;8:267–76.
[42] Lazzarin P, Zambardi R. A finite-volume-energy based approach to predict the static and fatigue behavior of components with sharp V-shaped notches. Int J Fract 2001;112:275–98.
[43] Lazzarin P, Berto F, Zappalorto M. Rapid calculations of notch stress intensity factors based on averaged strain energy density from coarse meshes: Theoretical bases and applications. Int J Fatigue 2010;32:1559–67.
[44] Nisitani H, Teranishi T. K_I value of a circumferential crack emanating from an ellipsoidal cavity obtained by the crack tip stress method in FEM. In: Guagliano M, Aliabadi MH, editors. Proc. 2nd Int. Conf. Fract. damage Mech., 2001, p. 141–6.
[45] Nisitani H, Teranishi T. K_I of a circumferential crack emanating from an ellipsoidal cavity obtained by the crack tip stress method in FEM. Eng Fract Mech 2004;71:579–85.
[46] Radaj D. State-of-the-art review on the local strain energy density concept and its relation to the J -integral and peak stress method. Fatigue Fract Eng Mater Struct 2015;38:2–28.
[47] Meneghetti G, Campagnolo A, Avalle M, Castagnetti D, Colussi M, Corigliano P, et al. Rapid evaluation of notch stress intensity factors using the peak stress method: Comparison of commercial finite element codes for a range of mesh patterns. Fatigue Fract Eng Mater Struct 2018;41.
[48] Campagnolo A, Meneghetti G. Rapid estimation of notch stress intensity factors in 3D large-scale welded structures using the peak stress method. MATEC Web Conf 2018;165.
[49] Lazzarin P, Tovo R. A unified approach to the evaluation of linear elastic stress fields in the neighborhood of cracks and notches. Int J Fract 1996;78:3–19.
[50] Lazzarin P, Berto F. Some expressions for the strain energy in a finite volume surrounding the root of blunt V-notches. Int J Fract 2005;135:161–85.
[51] Yung JY, Lawrence F V. Predicting the fatigue life of welds under combined bending and torsion. In: Brown M, Miller K, editors. Biaxial multiaxial fatigue EGF 3., London: Mechanical Engineering Publications; 1989, p. 53–69.
[52] Bergonzoni M, Campagnolo A, Pellinghelli D, Riboli M, Spagnoli A, Meneghetti G. Experimental tests and fatigue strength assessment of a scotch yoke valve actuator. Procedia Eng., vol. 213, 2018, p. 58–68.
[53] Meneghetti G, Campagnolo A, Menegalli A, Pagin L, Babini V, Dabala M, et al. Multiaxial fatigue assessment of a structural steel joint according to the peak stress method (only presentation). Int. Fatigue Congr. Fatigue 2018, Poitiers (France): 2018.
[54] Davi M. Local approaches applied to the fatigue strength assessment of laser welded joints (in Italian). University of Padova (Italy), 2018.
[55] Meneghetti G, Campagnolo A, Vormwald M, Shams E. The peak stress method applied to the fatigue assessment of tube-tube steel joints with weld ends under multiaxial loadings. 12th Int. Conf. Multiaxial Fatigue Fract., Bordeaux (France): 2019, *to be submitted*.

Figure

MULTIAXIAL FATIGUE ASSESSMENT OF WELDED STEEL DETAILS ACCORDING TO THE PEAK STRESS METHOD: INDUSTRIAL CASE STUDIES

Giovanni Meneghetti[1*], Alberto Campagnolo[1], Vittorio Babini[2], Matteo Riboli[3,4], Andrea Spagnoli[4]

[1] Department of Industrial Engineering, University of Padova, Via Venezia, 1 – 35131 Padova (Italy)
[2] Zamperla Spa, Via Monte Grappa 15/17, 36077, Altavilla Vicentina (Italy)
[3] Limitorque Fluid Power System, Flowserve S.r.l., Via Belizzi 40/42, 29122, Piacenza (Italy)
[4] Department of Engineering and Architecture, University of Parma, Parco Area delle Scienze 181/A, 43124, Parma (Italy)

* Corresponding author: giovanni.meneghetti@unipd.it, tel. 0039 049 8276751, fax 0039 049 8276785

CAPTIONS TO FIGURES AND TABLES

Figure 1: Assumptions of the NSIF-based approach in fatigue design of welded joints. The sharp V-notch opening angle 2α is typically 0° at the weld root and 135° at the weld toe.

Figure 2: Cylindrical reference system centred at the weld toe and stress components of a typical tube-to-flange welded joint geometry subjected to multiaxial bending and torsion loading.

Figure 3: Typical 2D FE mesh to apply the PSM according to Eqs. (8)-(10) in the case of a tube-to-flange fillet welded joint (from [31]). Four-node, quadrilateral, harmonic PLANE 25 elements available in Ansys® Element Library were adopted to generate the free mesh. Axes have been renamed, in that Y must be the axisymmetric direction in Ansys® models.

Figure 4: The structural volume to calculate the averaged SED [50] at a radiused weld toe ($\rho \neq 0$) according to Eq. (7).

Figure 5: Residual stress components and path for residual stress measurement in full-penetration welded joints (model 1 of Table 3).

Figure 6: Residual stresses in full-penetration welded joints (model 1 of Table 3) in the as-welded conditions by the X-ray diffraction method. (a) axial σ_{xx} and (b) hoop σ_{zz} residual stress components along the path shown in Fig. 5.

Figure 7: Residual stresses in full-penetration welded joints (model 1 of Table 3) during the fatigue life. (a) and (b) as-welded and (c) and (d) stress-relieved conditions.

Figure 8: (a) A pair of full-penetration joints (model 1 of Table 3) tested simultaneously in the axial fatigue test machine. (b) Load and restraints applied to the specimens. (c) A pair of fillet-welded joints (model 2 of Table 3) tested simultaneously in the axial fatigue test machine. (d) Load and restraints applied to the specimens.

Figure 9: Maximum displacement S_{max} measured by the MTS controller during a fatigue test for (a) full-penetration and (b) fillet-welded joints. Definition of technical crack initiation life N_i and fatigue life to failure N_f.

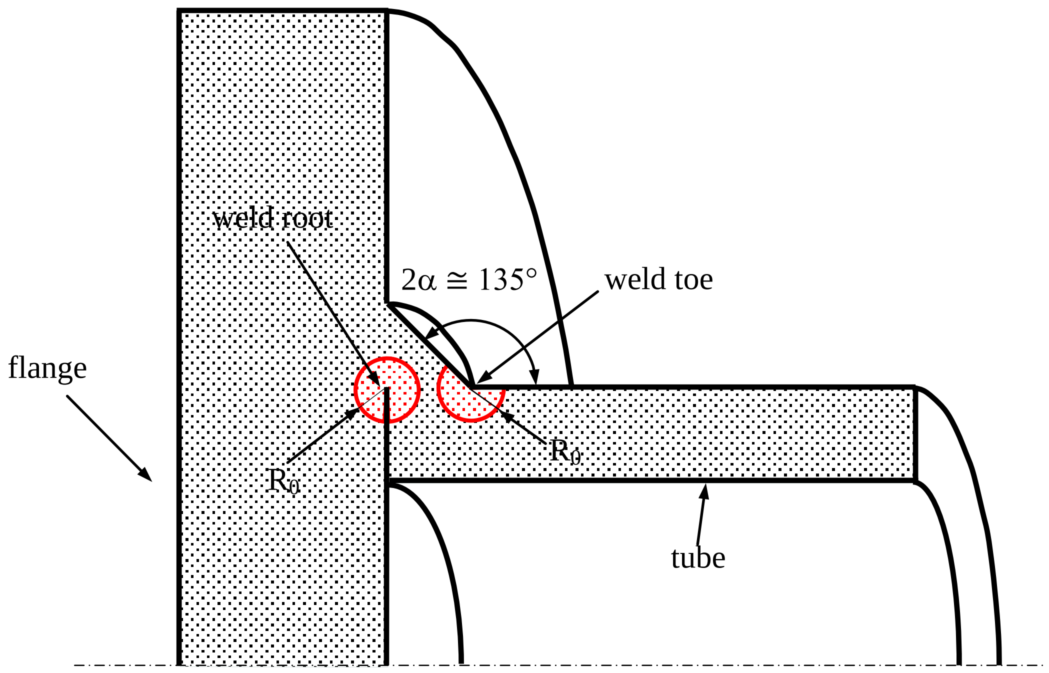

Figure 1: Assumptions of the NSIF-based approach in fatigue design of welded joints. The sharp V-notch opening angle 2α is typically 0° at the weld root and 135° at the weld toe.

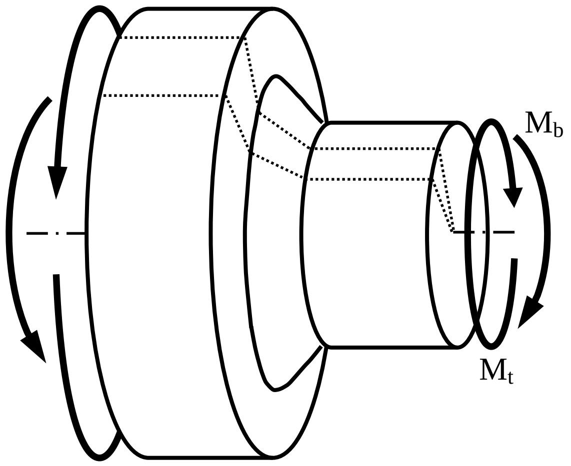

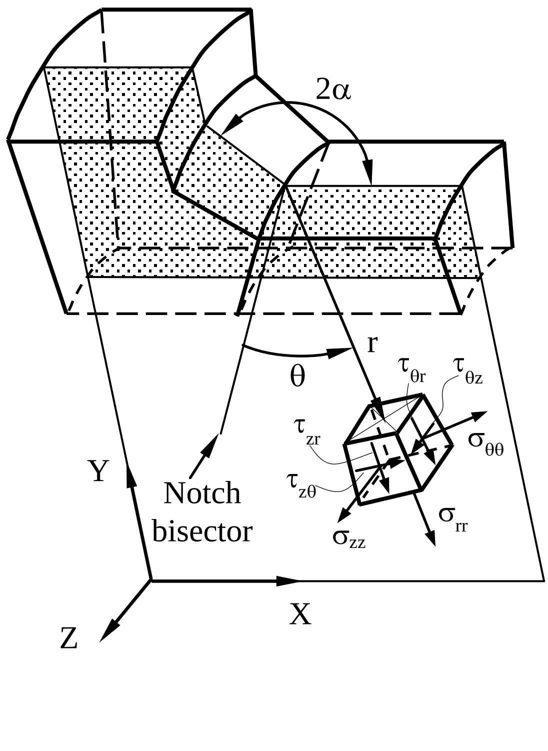

Figure 2: Cylindrical reference system centred at the weld toe and stress components of a typical tube-to-flange welded joint geometry subjected to multiaxial bending and torsion loading.

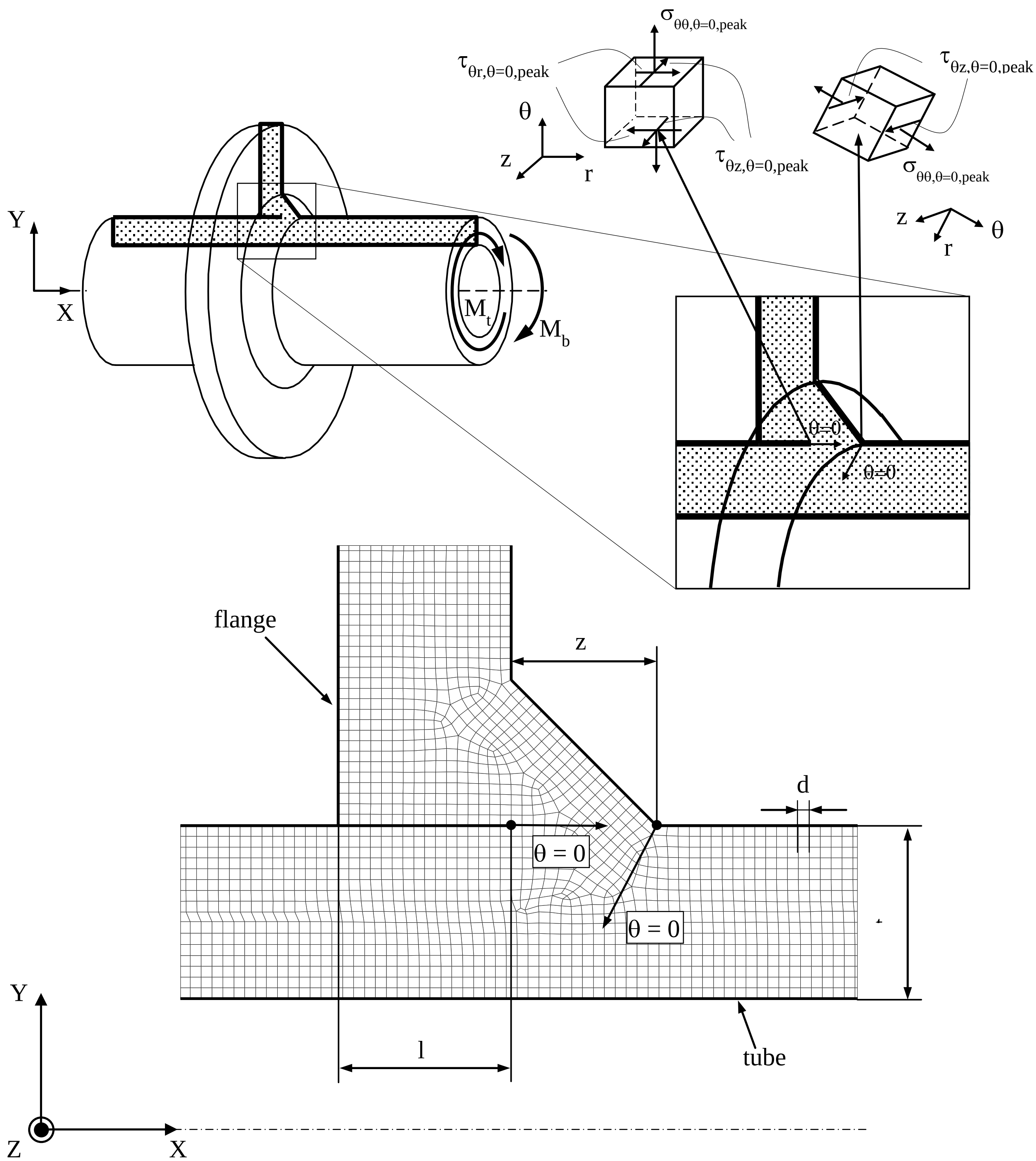

Figure 3: Typical 2D FE mesh to apply the PSM according to Eqs. (8)-(10) in the case of a tube-to-flange fillet welded joint (from [31]). Four-node, quadrilateral, harmonic PLANE 25 elements available in Ansys® Element Library were adopted to generate the free mesh. Axes have been renamed, in that Y must be the axisymmetric direction in Ansys® models.

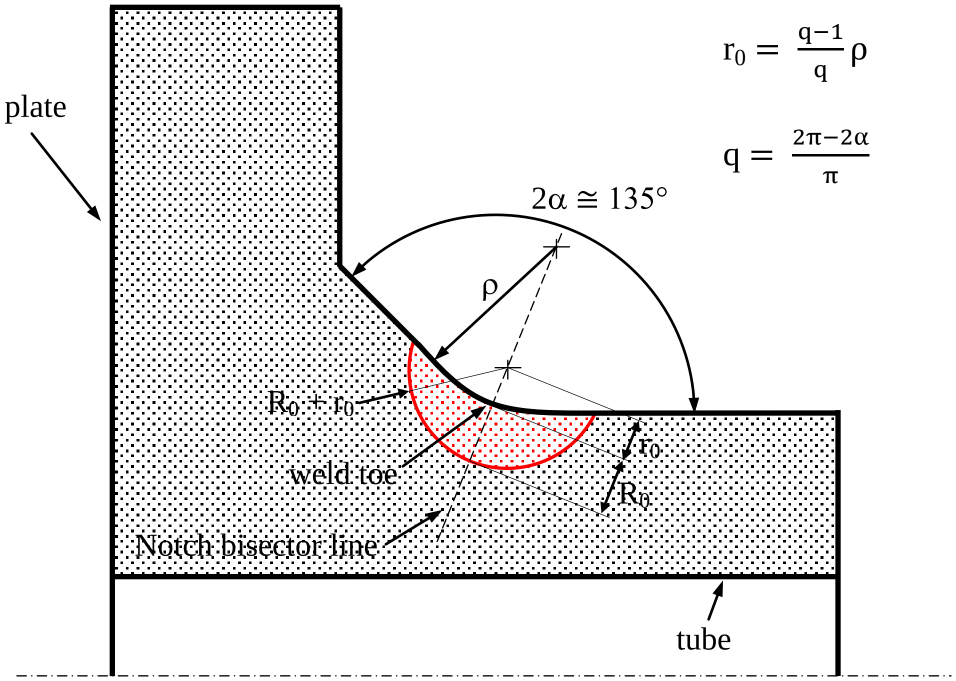

Figure 4: The structural volume to calculate the averaged SED [50] at a radiused weld toe ($\rho \neq 0$) according to Eq. (7).

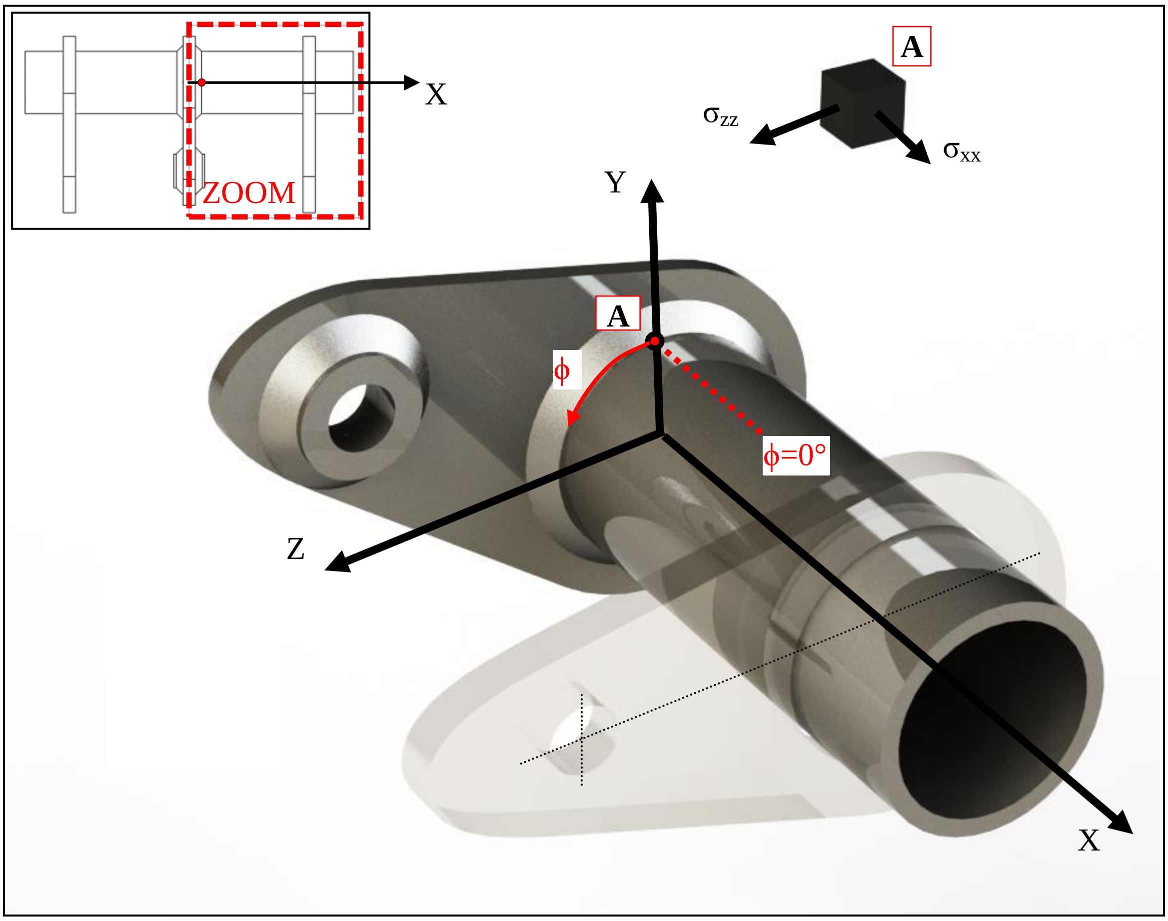

Figure 5: Residual stress components and path for residual stress measurement in full-penetration welded joints (model 1 of Table 3).

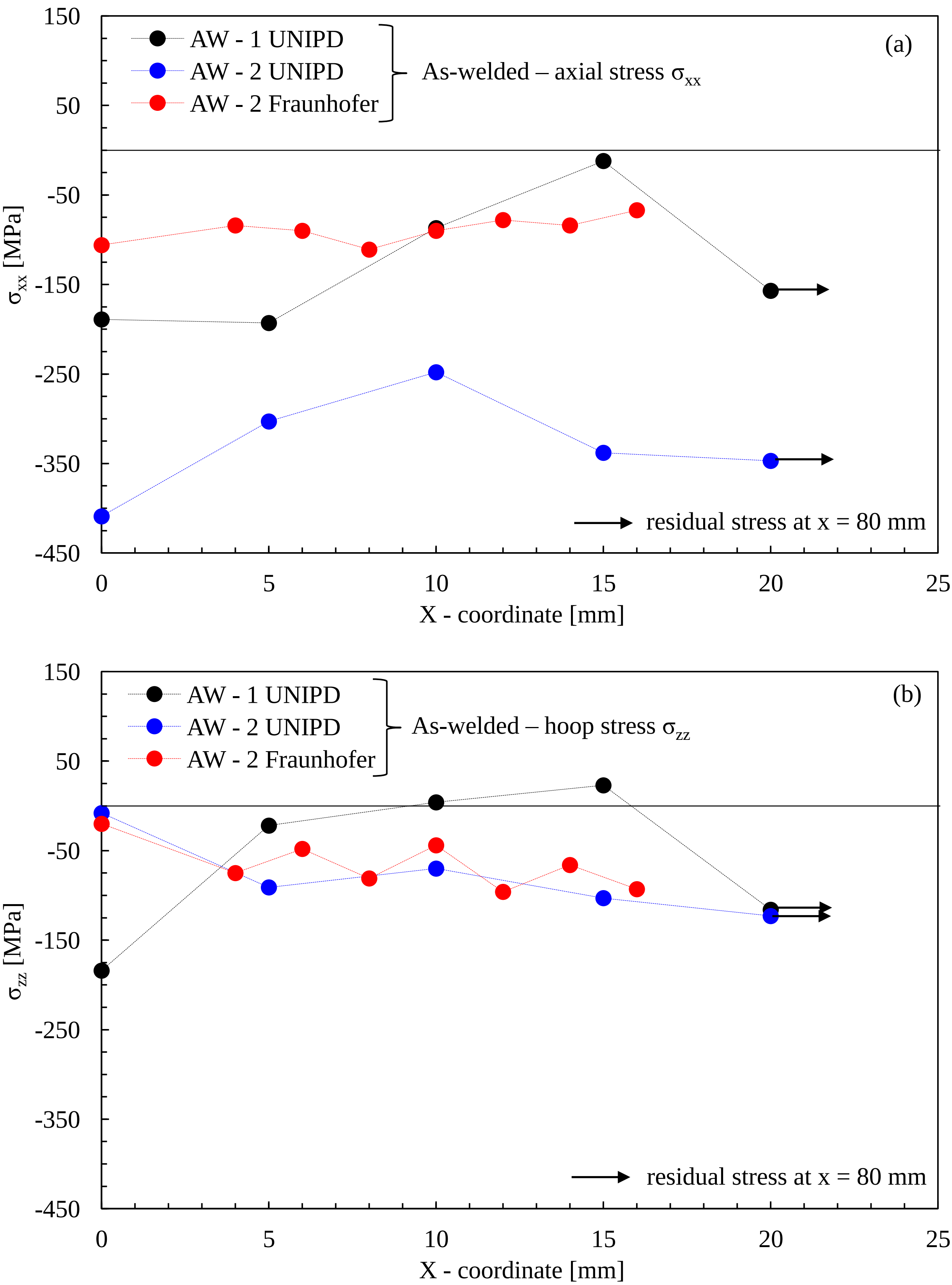

Figure 6: Residual stresses in full-penetration welded joints (model 1 of Table 3) in the as-welded conditions by the X-ray diffraction method. (a) axial σ_{xx} and (b) hoop σ_{zz} residual stress components along the path shown in Fig. 5.

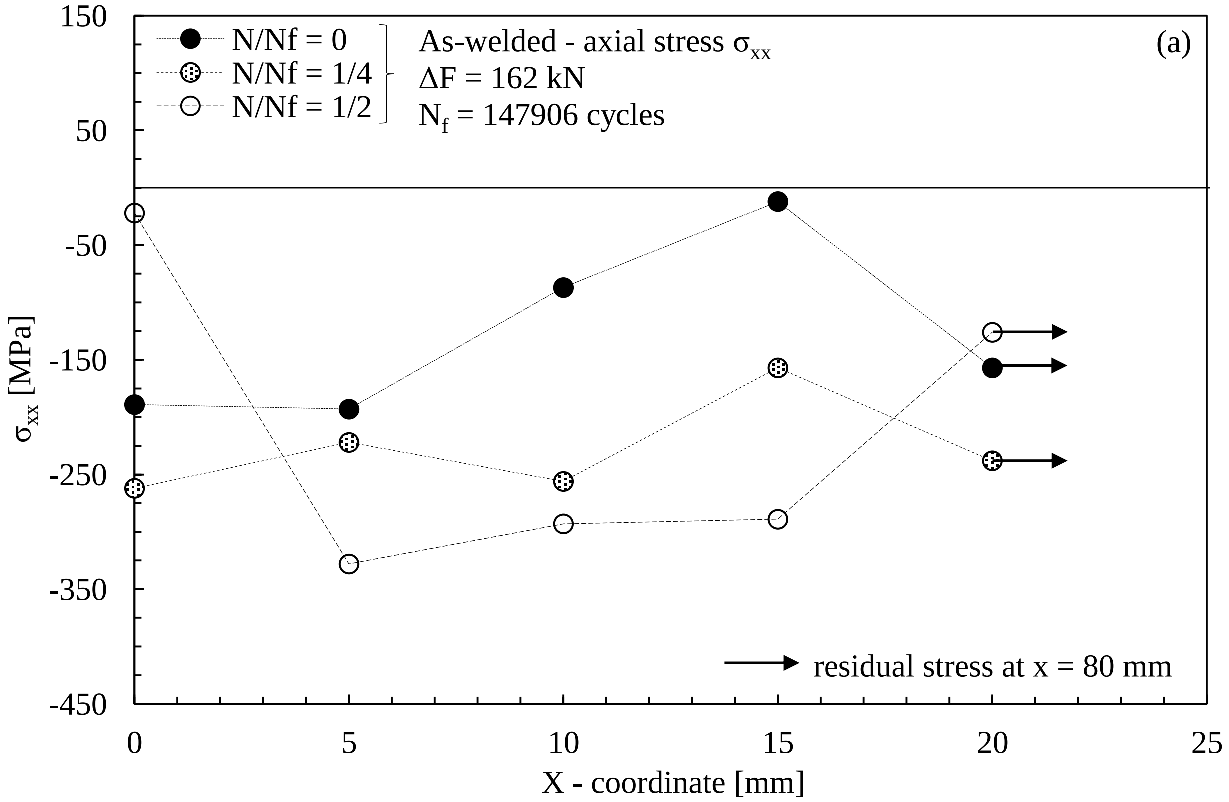

N/Nf = 0
N/Nf = 1/4
N/Nf = 1/2
As-welded - axial stress σxx
ΔF = 162 kN
Nf = 147906 cycles
(a)
residual stress at x = 80 mm
σxx [MPa]
X - coordinate [mm]

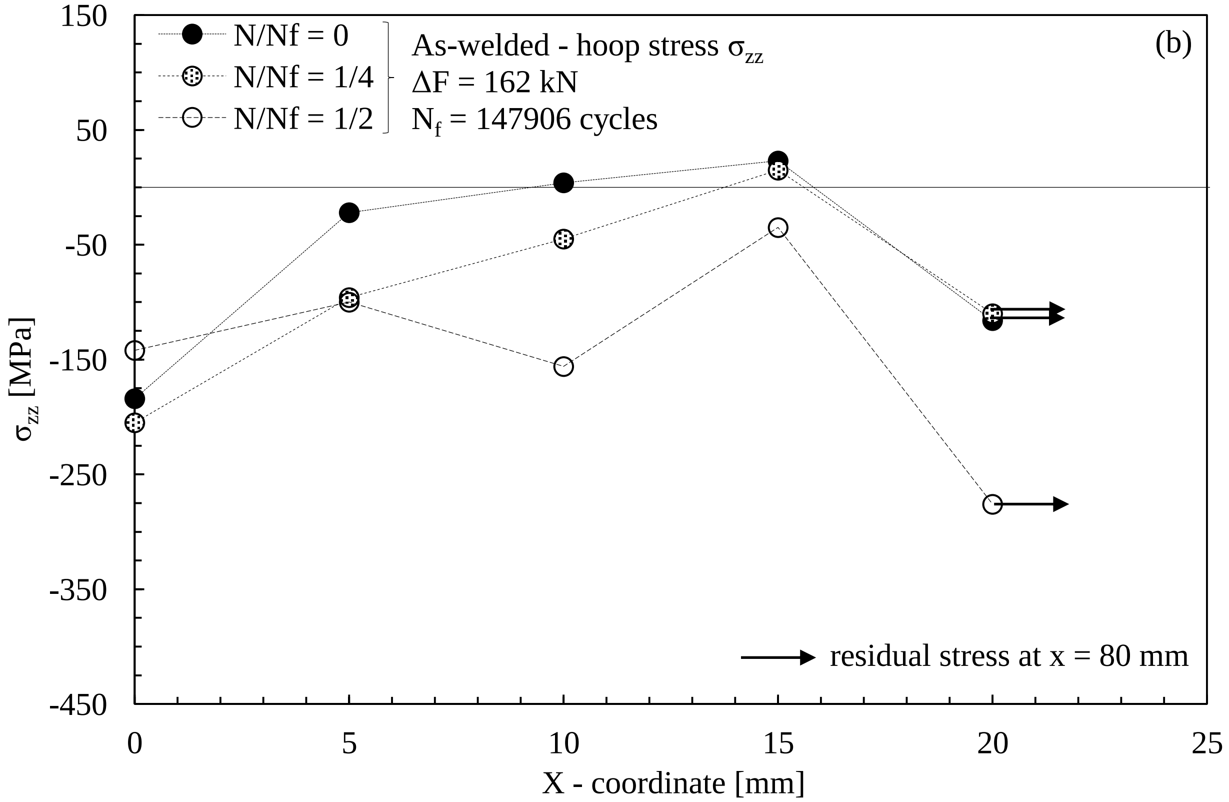

N/Nf = 0
N/Nf = 1/4
N/Nf = 1/2
As-welded - hoop stress σzz
ΔF = 162 kN
Nf = 147906 cycles
(b)
residual stress at x = 80 mm
σzz [MPa]
X - coordinate [mm]

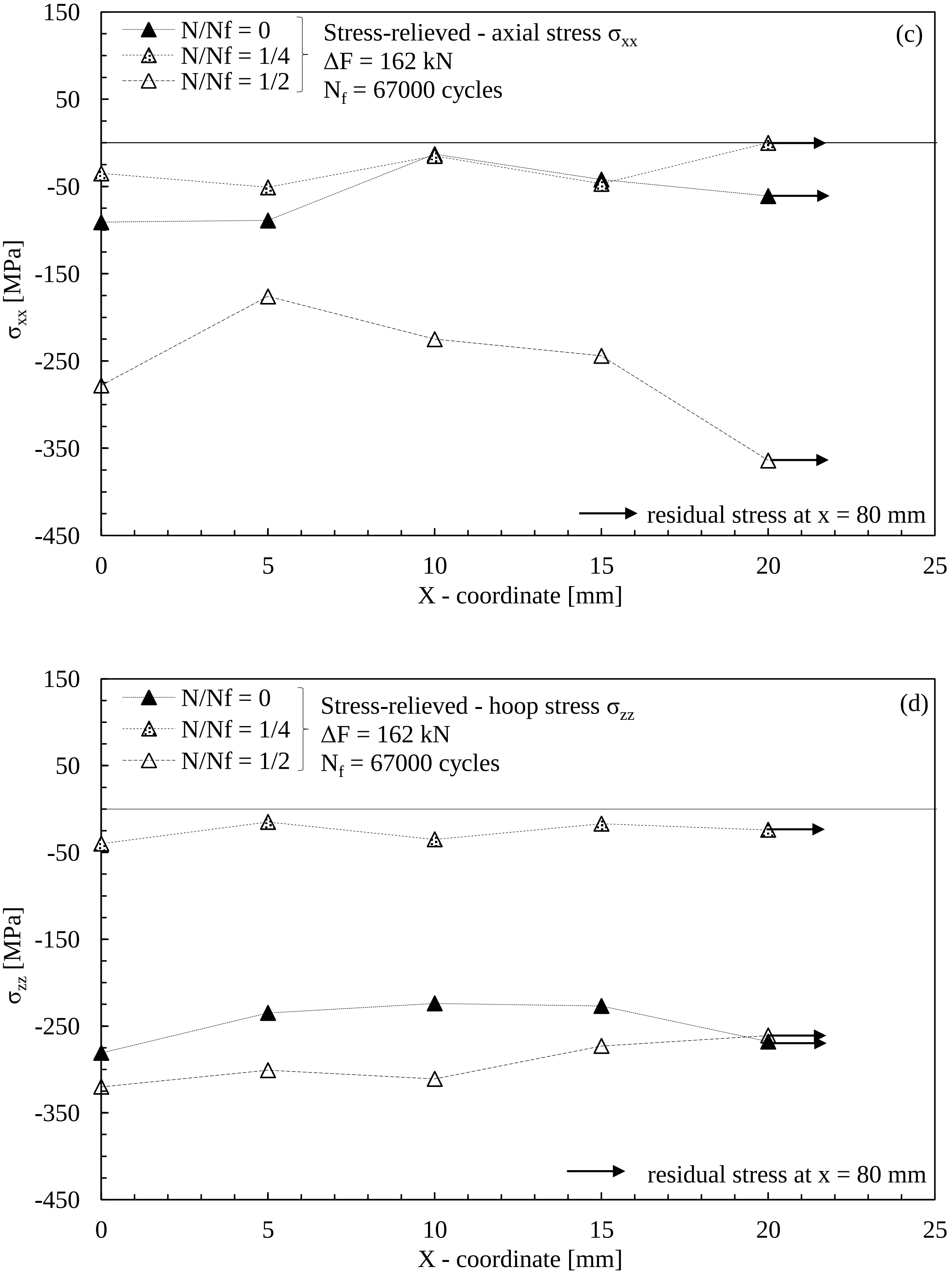

Figure 7: Residual stresses in full-penetration welded joints (model 1 of Table 3) during the fatigue life. (a) and (b) as-welded and (c) and (d) stress-relieved conditions.

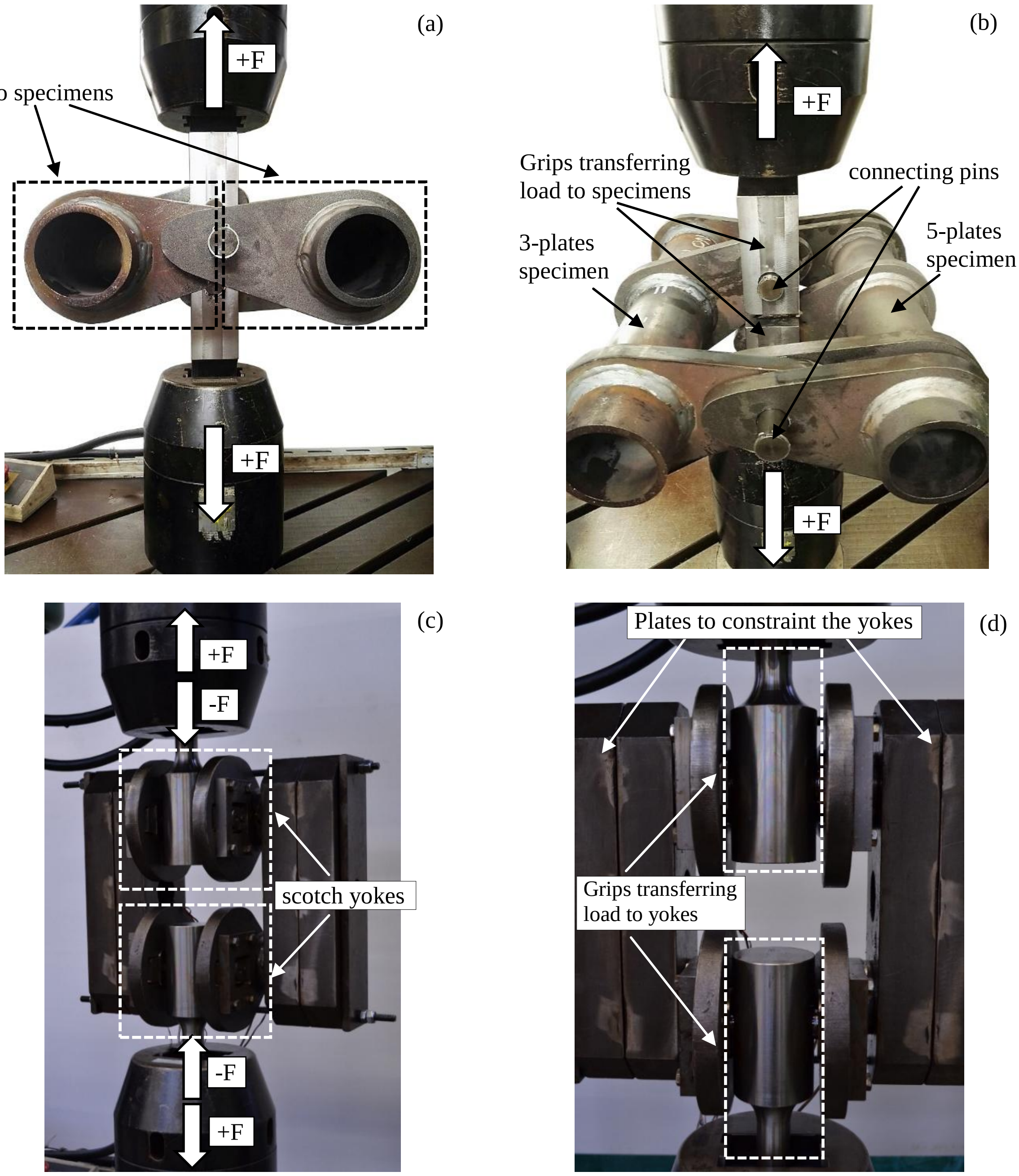

Figure 8: (a) A pair of full-penetration joints (model 1 of Table 3) tested simultaneously in the axial fatigue test machine. (b) Load and restraints applied to the specimens. (c) A pair of fillet-welded joints (model 2 of Table 3) tested simultaneously in the axial fatigue test machine. (d) Load and restraints applied to the specimens.

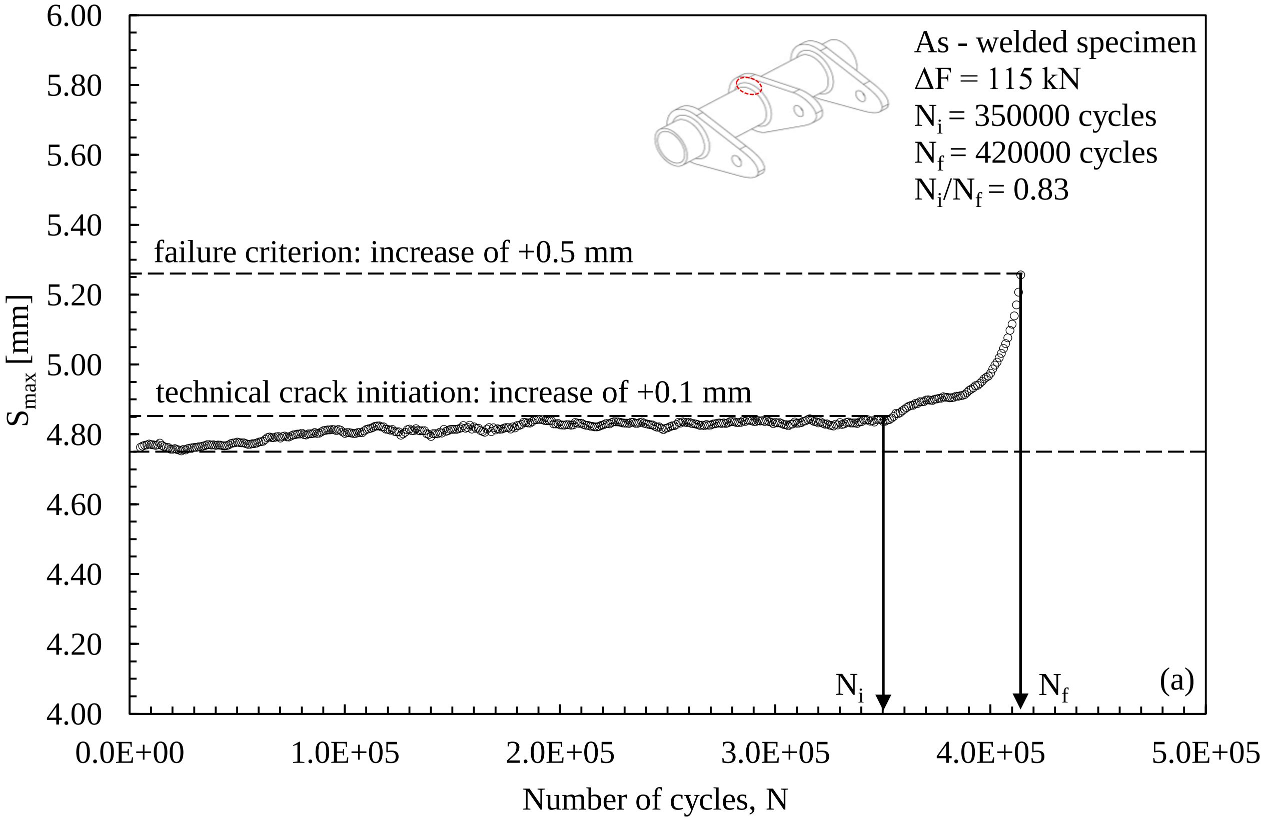

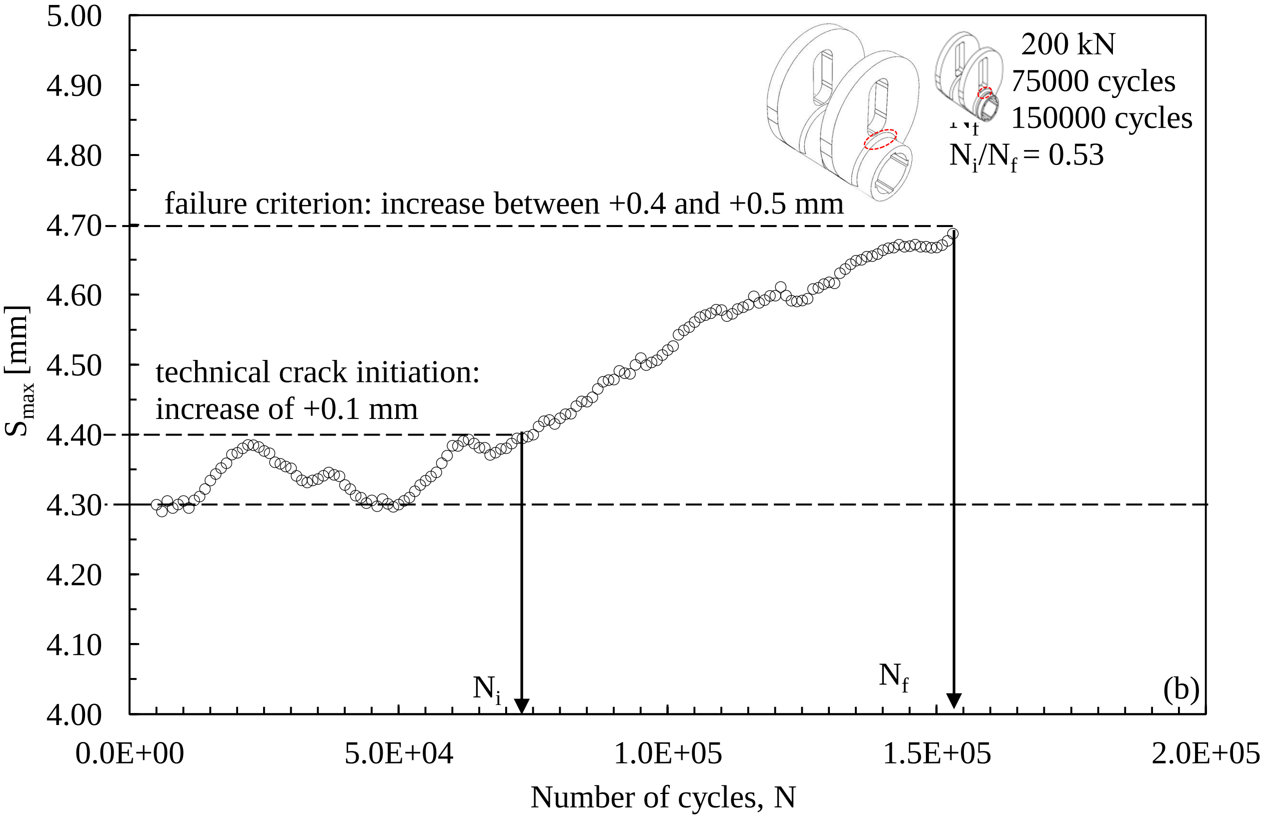

Figure 9: Maximum displacement S_{max} measured by the MTS controller during a fatigue test for (a) full-penetration and (b) fillet-welded joints. Definition of technical crack initiation life N_i and fatigue life to failure N_f.

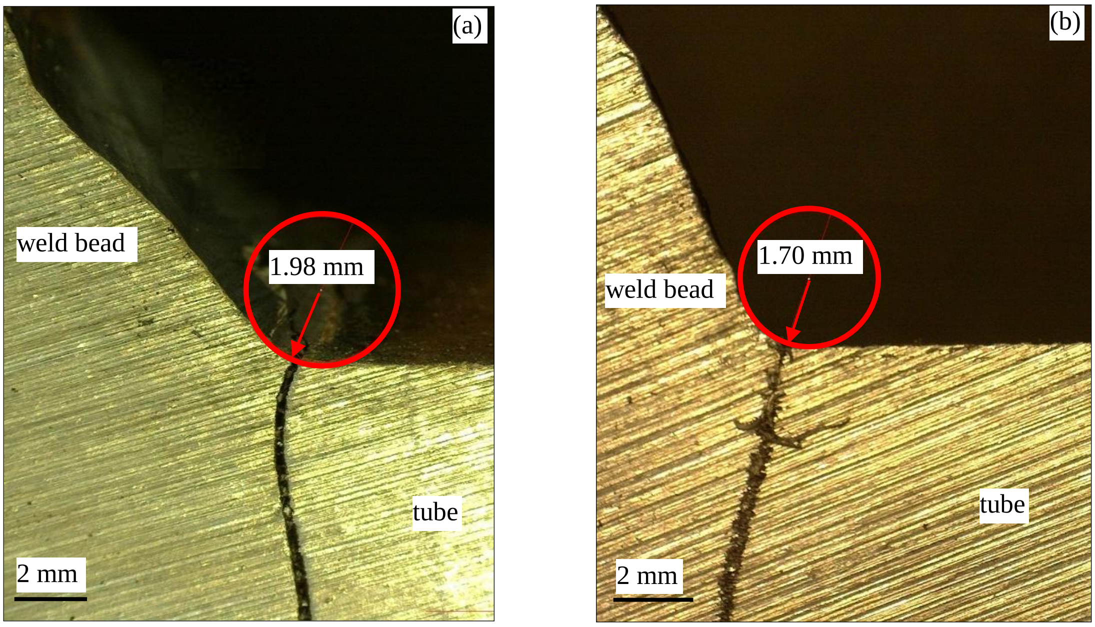

Figure 10: Weld toe radius at the tube side of full-penetration welded joints: (a) AW, ΔF = 132 kN, N_i = 305000 cycles and N_f = 320000 cycles; (b) SR, ΔF = 162 kN, N_i = 49000 cycles and N_f = 67000 cycles.

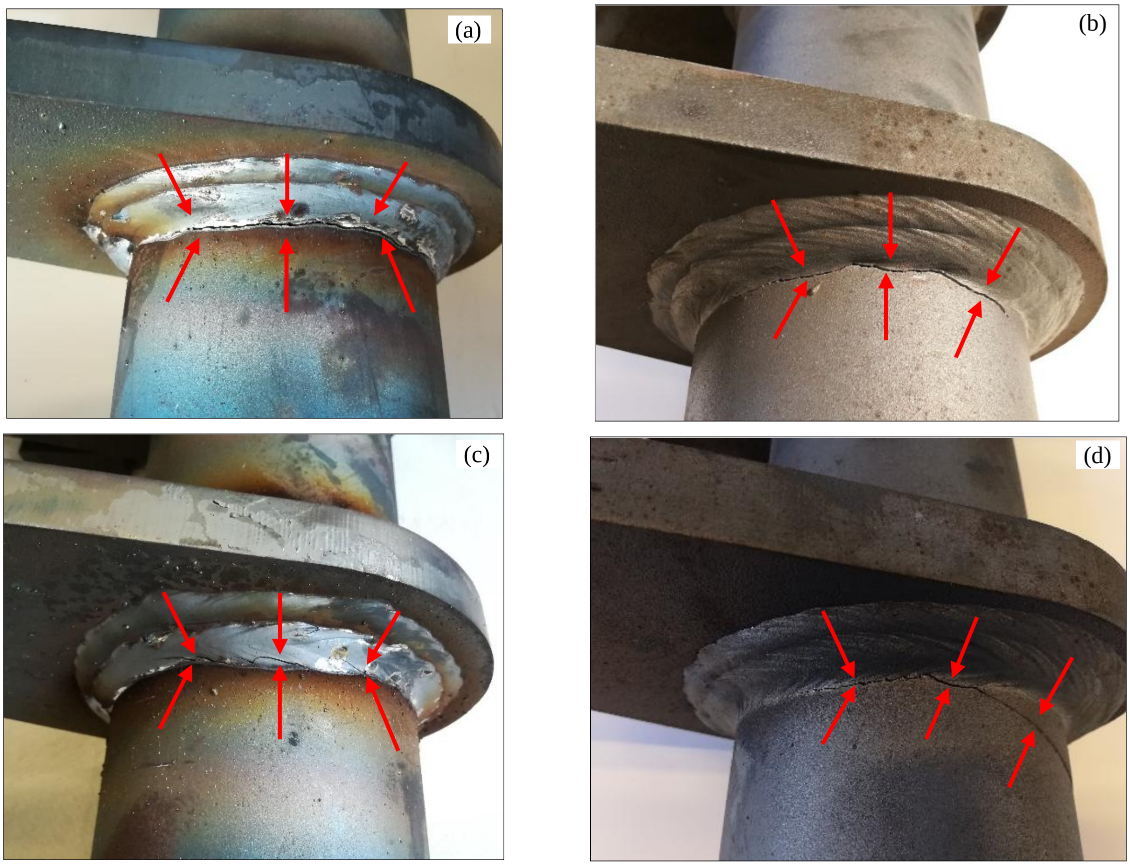

Figure 11: Fatigue cracks in full-penetration welded joints (model 1 of Table 3). (a) AW, ΔF = 132 kN, $N_i \approx N_f$ = 145000 cycles; (b) SR, ΔF = 132 kN, N_i = 95000 cycles and N_f = 110000 cycles; (c) AW, ΔF = 115 kN, N_i = 350000 cycles and N_f = 420000 cycles; (d) SR, ΔF = 115 kN, N_i = 335000 cycles and N_f = 383000 cycles.

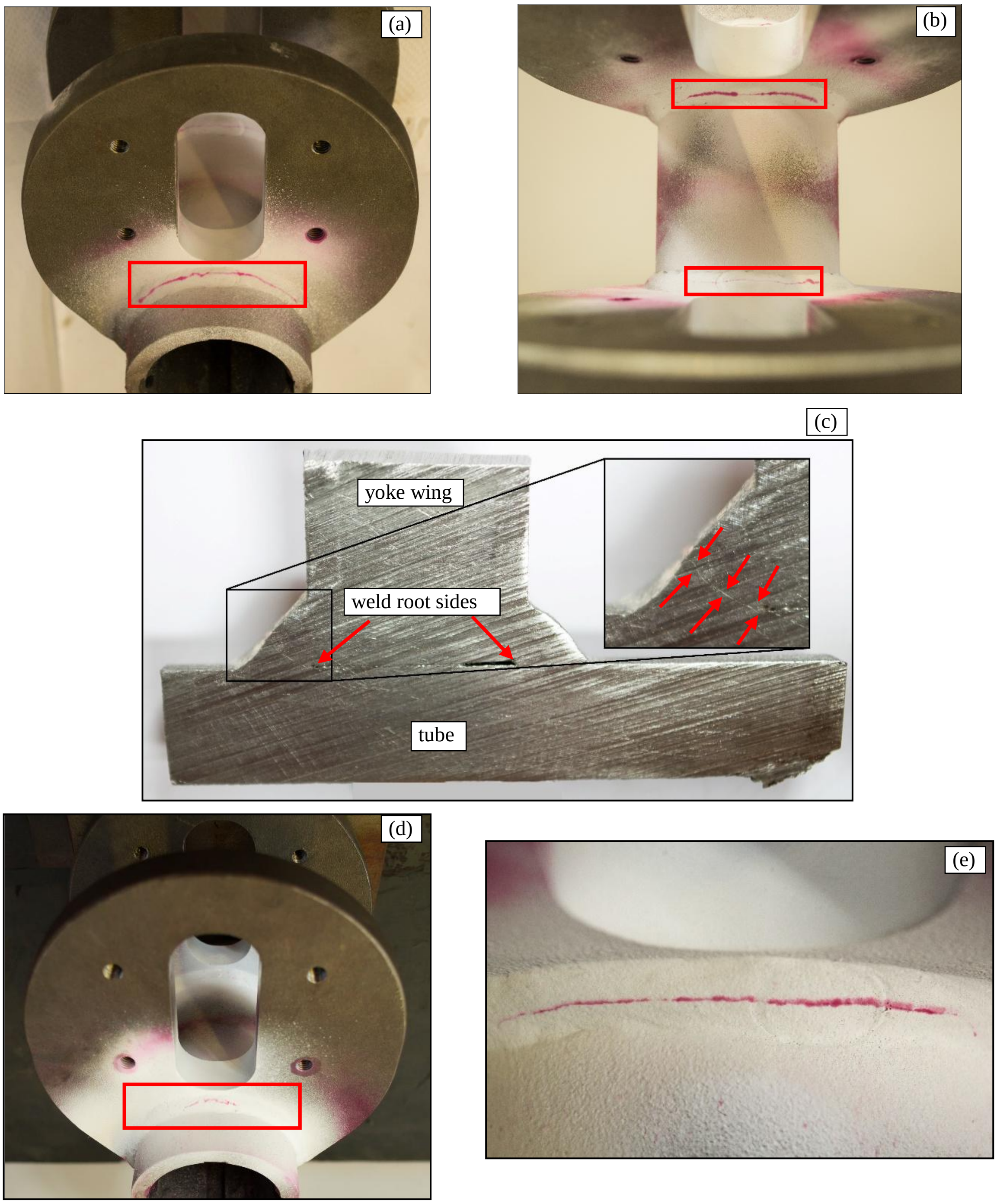

Figure 12: Fatigue crack paths analysed by means of dye penetrant inspections in fillet-welded joint (model 2 of Table 3): fatigue crack initiated at weld root and emerged at the weld bead surface: (a), (b) and (c) ΔF = 200 kN, N_i = 78000 cycles and N_f = 150000 cycles; (d) and (e) ΔF = 150 kN, N_i = 350000 cycles and N_f = 693800 cycles.

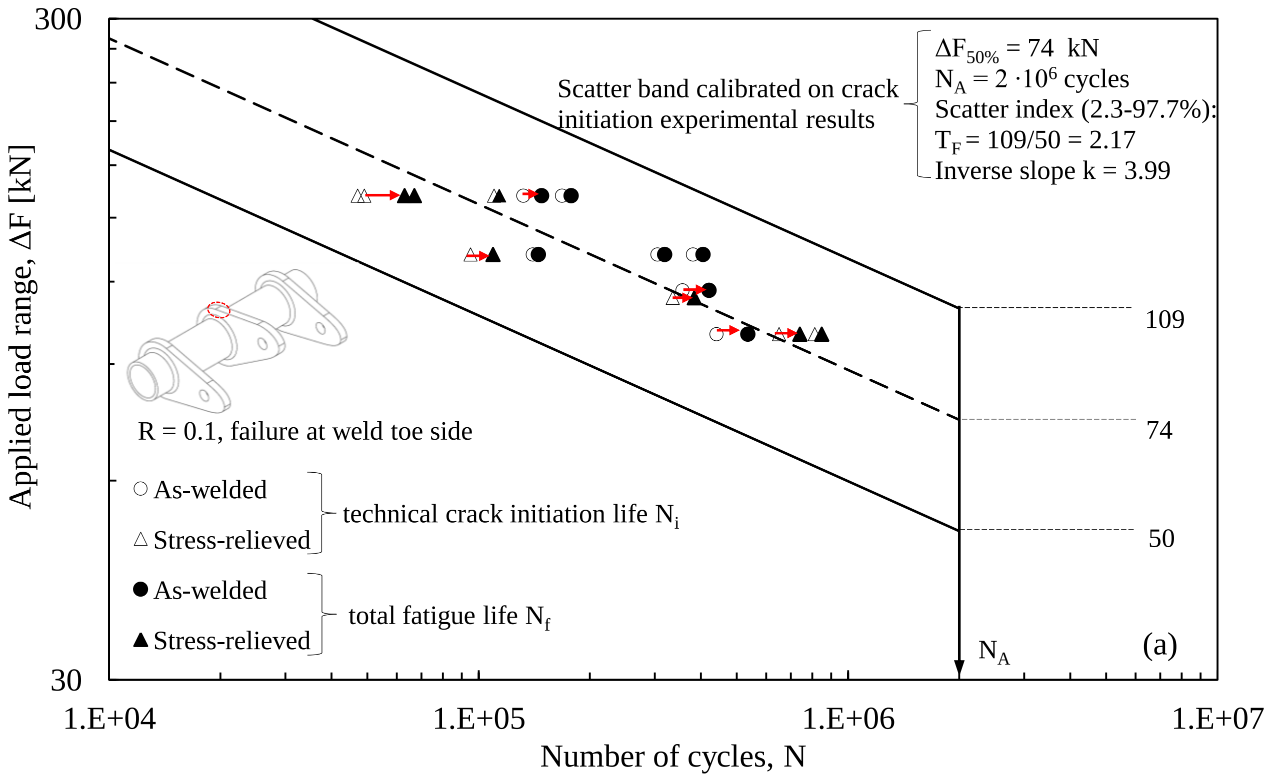

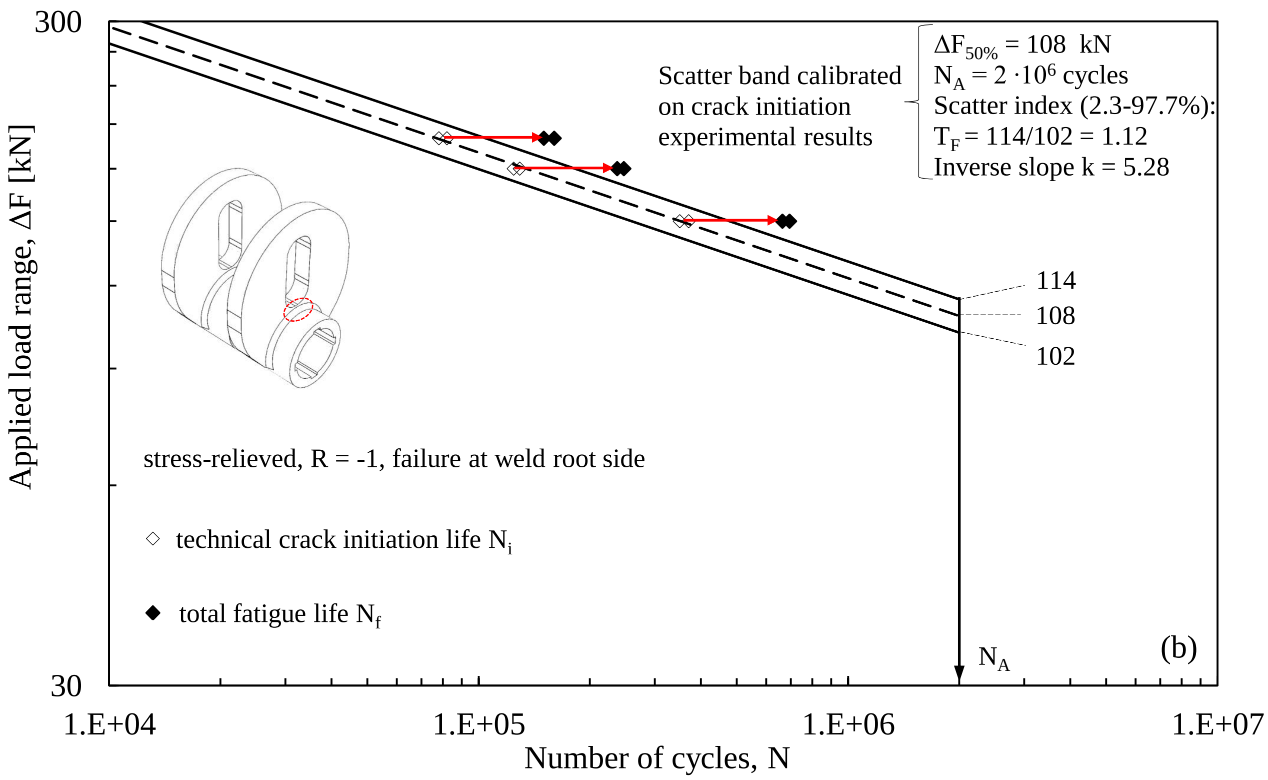

Figure 13: Experimental fatigue results in terms of number of cycles versus the applied load range. (a) full-penetration and (b) fillet-welded joints. Scatter bands calculated with 95% confidence level. Open markers refer to the fatigue life N_i to technical crack initiation (see definition in Table 5), filled markers refer to the total fatigue life N_f (see definition in Table 5).

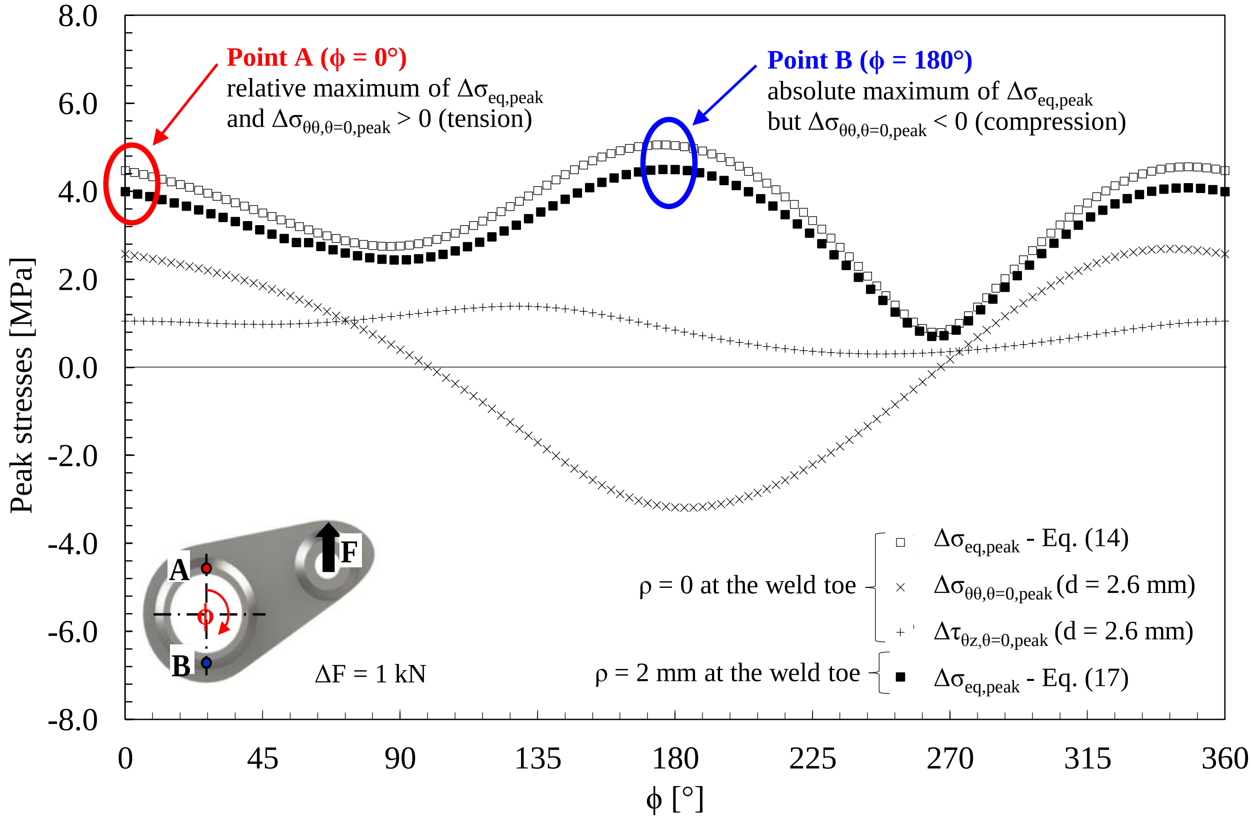

Figure 14: Estimation of the crack initiation point in full-penetration welded joints (model 1 of Table 3) based on the distribution of the equivalent peak stress along the weld toe line. Equivalent peak stress evaluated from Eq. (14) by assuming a sharp V-notch (ρ = 0) and from Eq. (17) assuming a radiused notch (ρ = 2 mm).

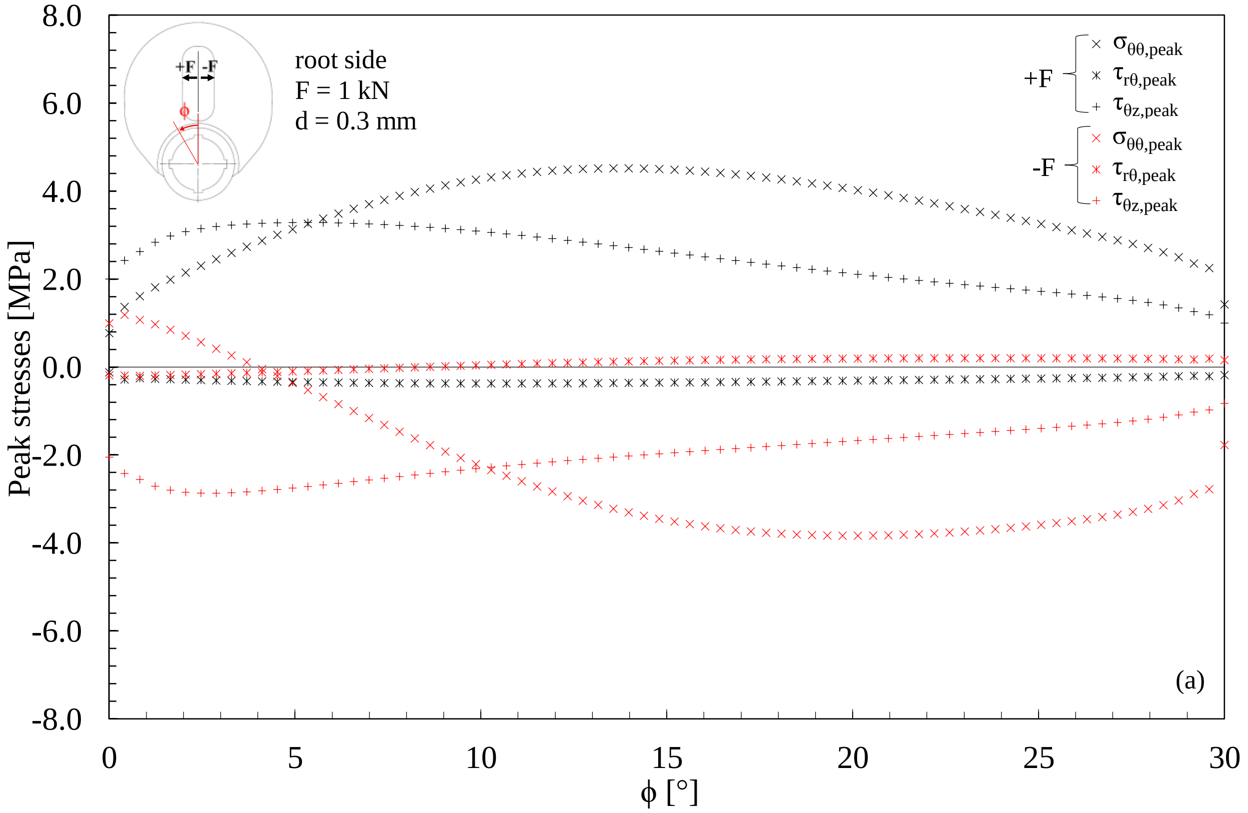

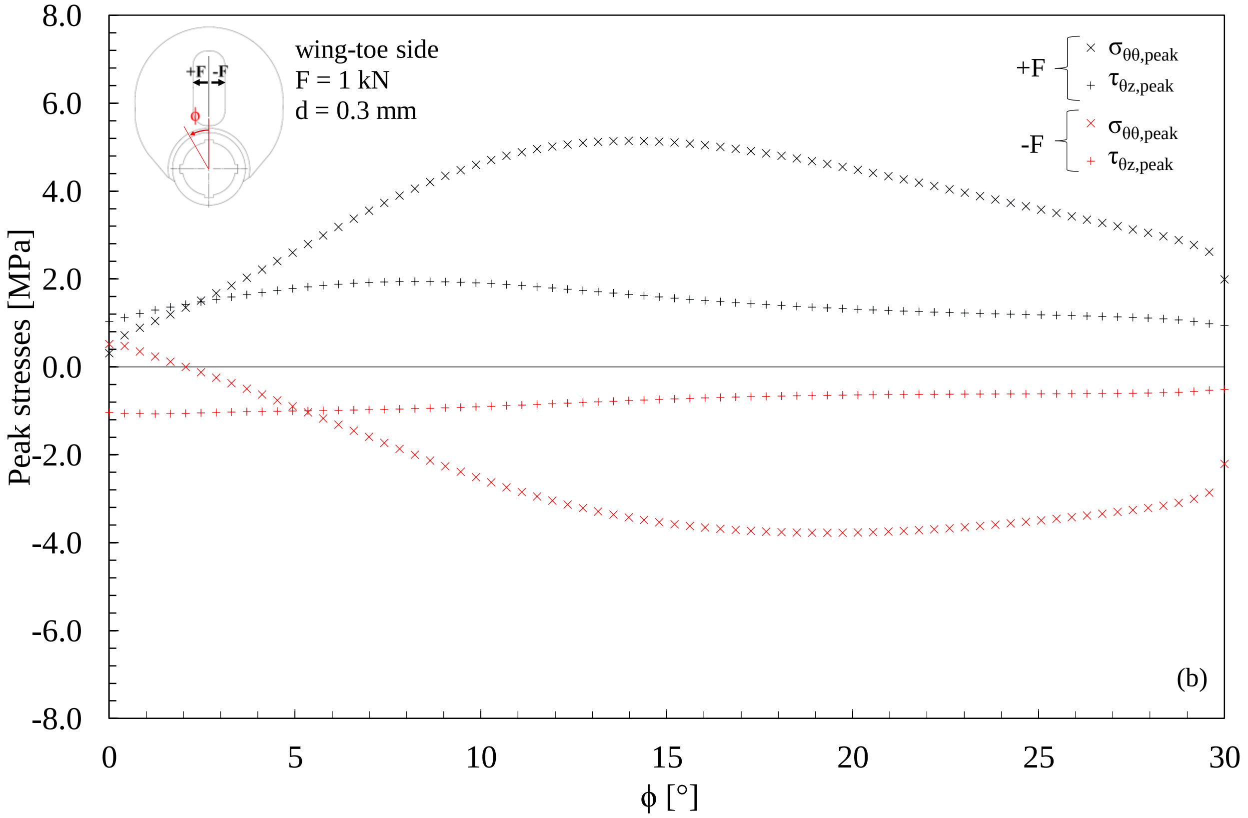

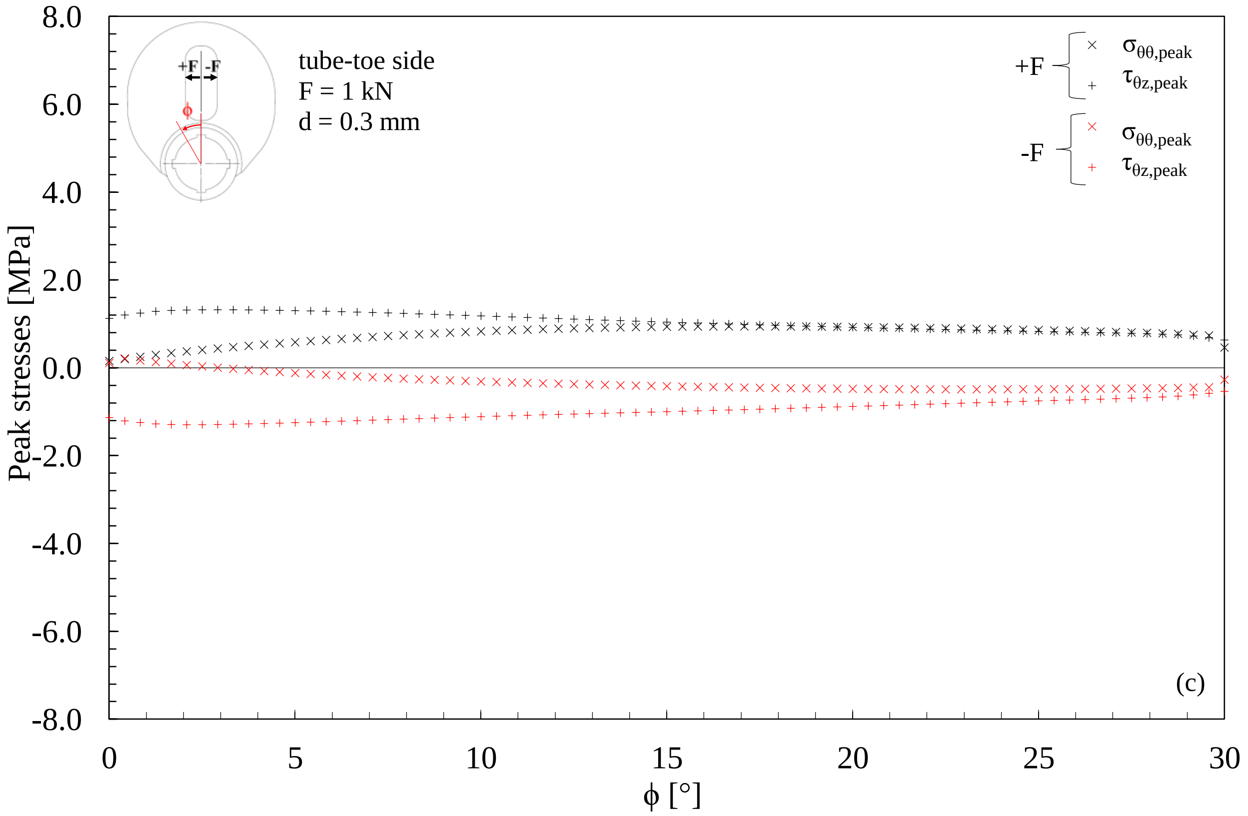

Figure 15: Distribution of the mode I, mode II and mode III peak stresses in the scotch yoke joint (model 2 of Table 3) along the (a) weld root, (b) wing-toe and (c) tube-toe lines.

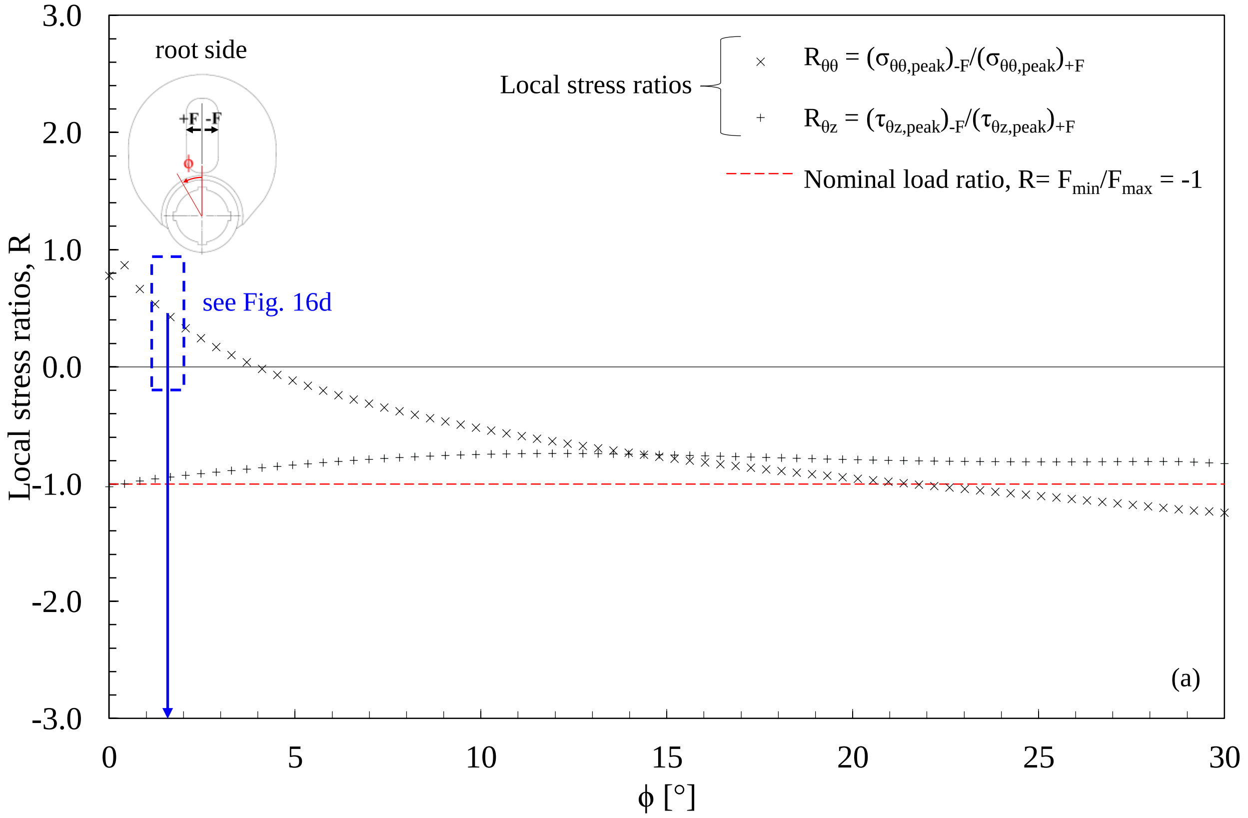
root side
+F -F
ϕ
Local stress ratios
$R_{\theta\theta} = (\sigma_{\theta\theta,peak})_{-F}/(\sigma_{\theta\theta,peak})_{+F}$
$R_{\theta z} = (\tau_{\theta z,peak})_{-F}/(\tau_{\theta z,peak})_{+F}$
Nominal load ratio, $R= F_{min}/F_{max} = -1$
see Fig. 16d
Local stress ratios, R
ϕ [°]
(a)

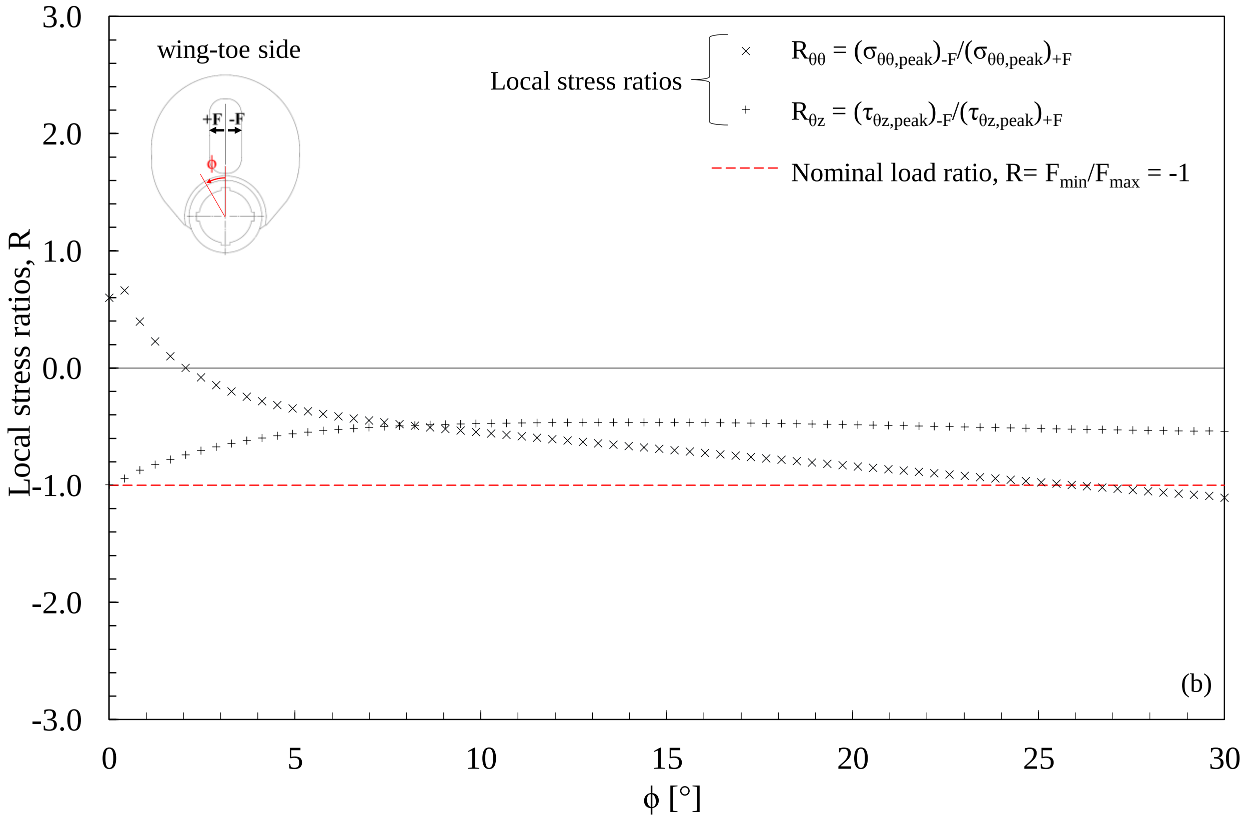
wing-toe side
+F -F
ϕ
Local stress ratios
$R_{\theta\theta} = (\sigma_{\theta\theta,peak})_{-F}/(\sigma_{\theta\theta,peak})_{+F}$
$R_{\theta z} = (\tau_{\theta z,peak})_{-F}/(\tau_{\theta z,peak})_{+F}$
Nominal load ratio, $R= F_{min}/F_{max} = -1$
Local stress ratios, R
ϕ [°]
(b)

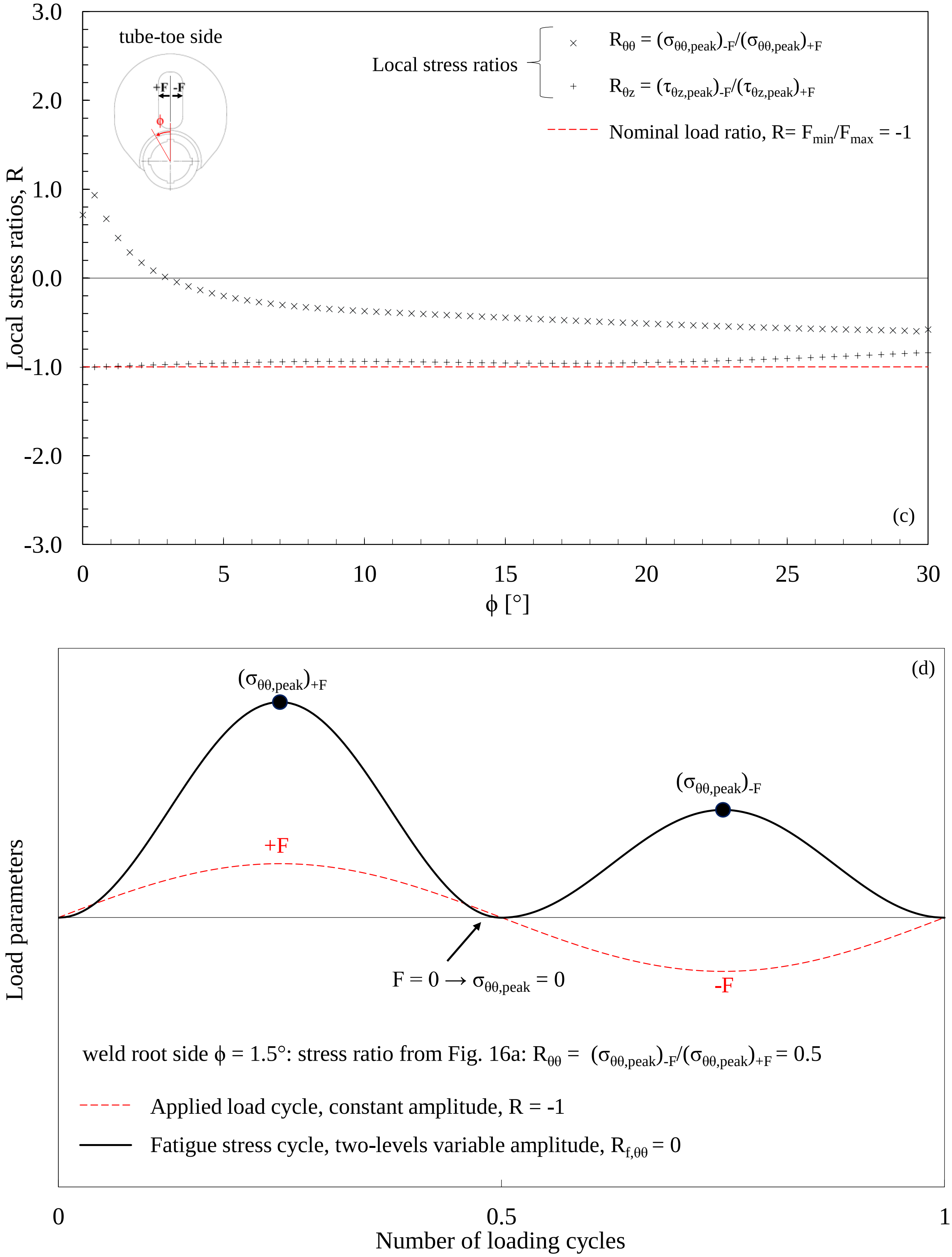

Figure 16: Distribution of the local stress ratios R of mode I and mode III peak stresses along (a) weld root, (b) wing-toe and (c) tube-toe lines (model 2 of Table 3). (d) Local fatigue stress ratio R_f of the mode I peak stress $\sigma_{\theta\theta,peak}$ in the region where $R_{\theta\theta} > 0$. The figure refers to the weld root at $\phi = 1.5°$.

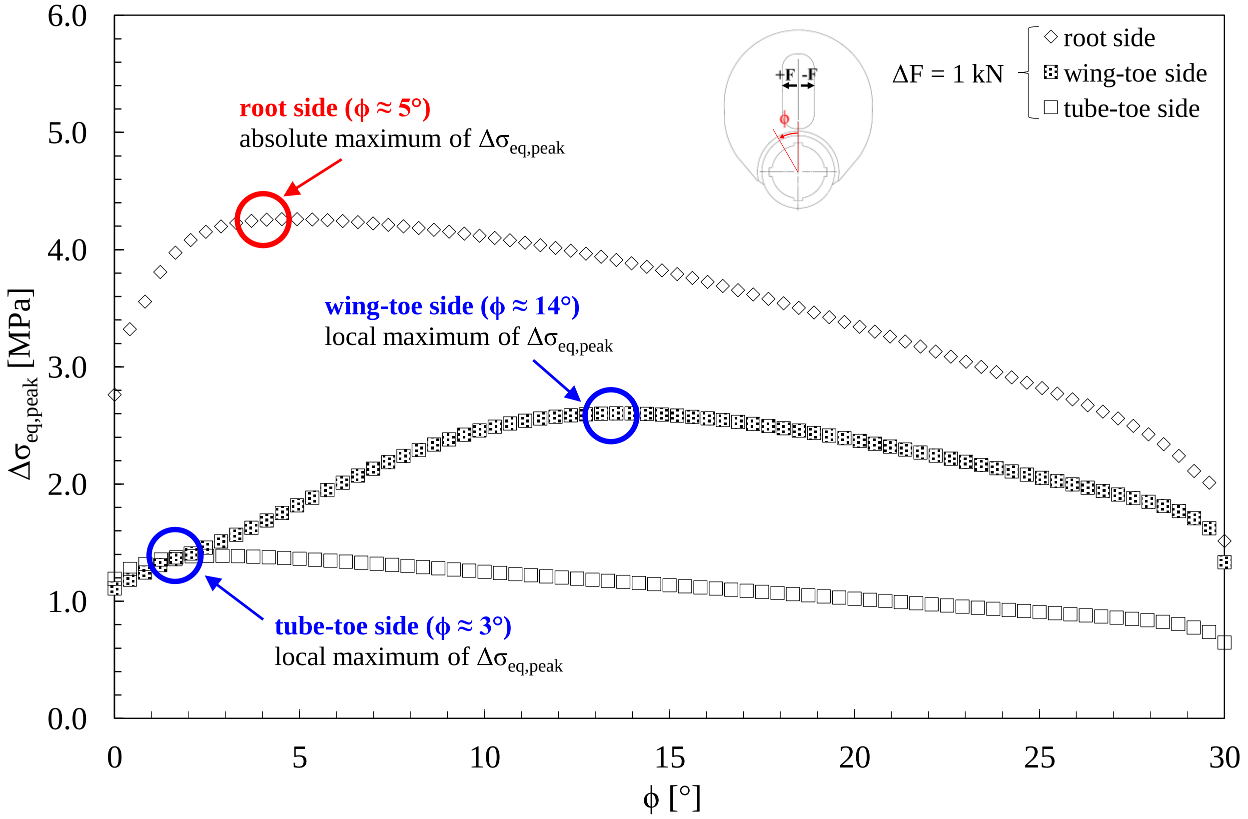

Figure 17: Estimation of the crack initiation point in fillet-welded joints (model 2 of Table 3) based on the distribution of the equivalent peak stress along the weld root, wing-toe and tube-toe lines. Equivalent peak stress evaluated from Eq. (22) with the peak stresses reported in Fig. 15.

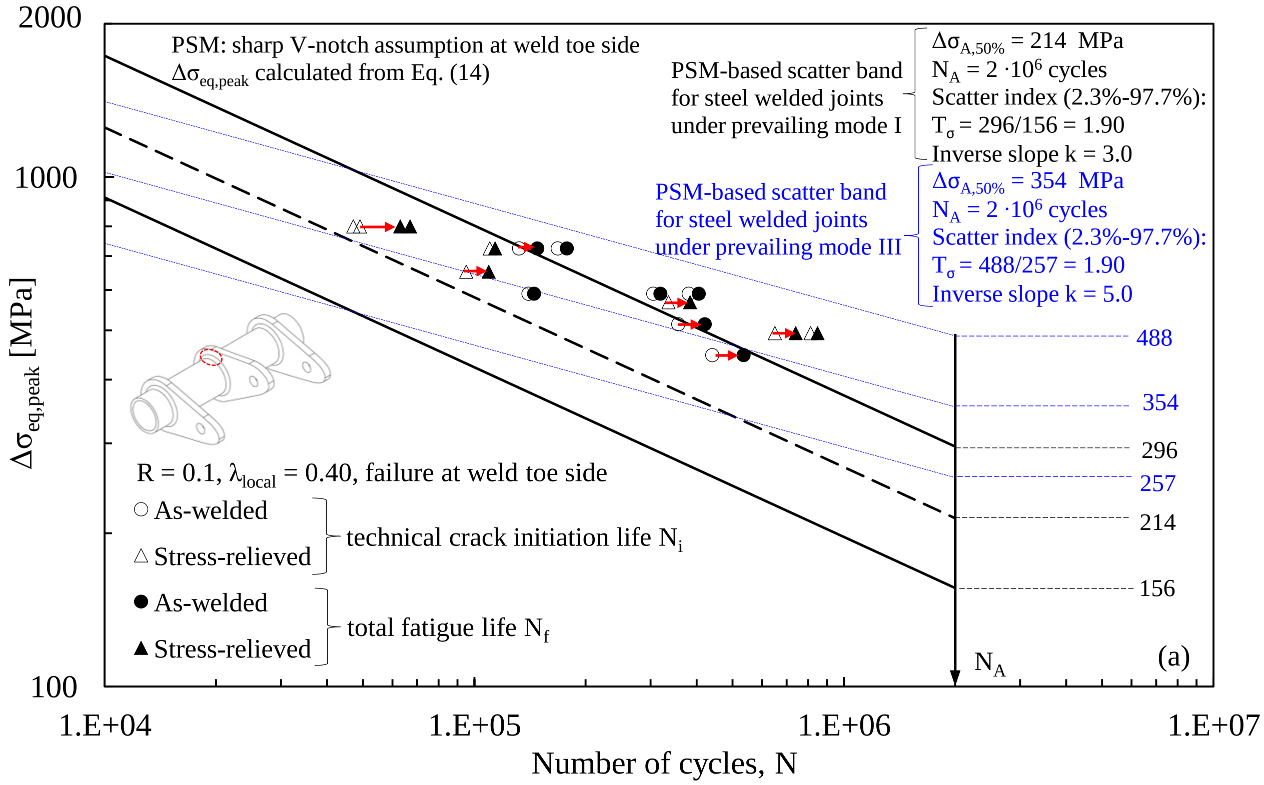

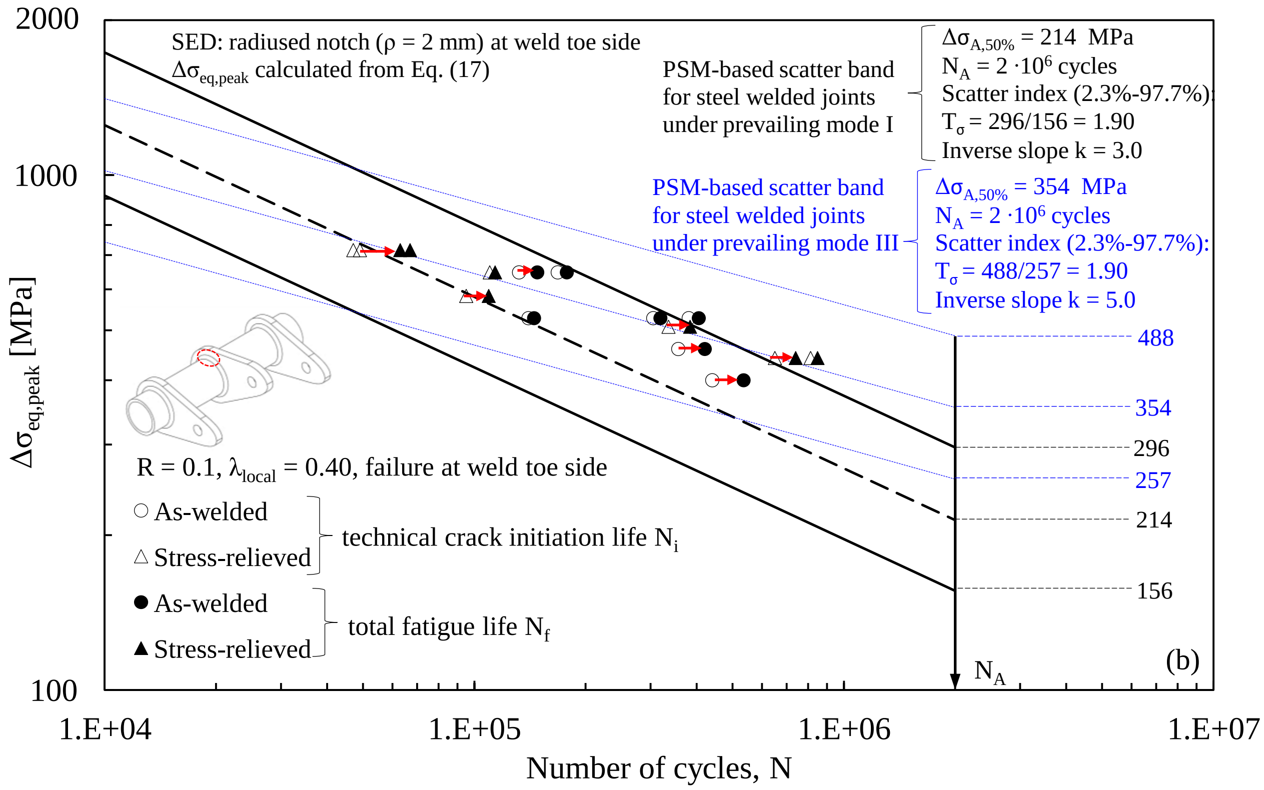

Figure 18: Fatigue assessment of toe failures in full-penetration structural steel welded joints (model 1 of Table 3) under combined bending-torsion in-phase loading according to the PSM. (a) sharp V-notch assumption and (b) a radiused notch with ρ = 2 mm at weld toe. The design scatter band was previously calibrated in Ref. [26]. For comparison purposes, the figure reports also the design scatter band previously calibrated in Ref. [25] for steel welded joint under pure mode III loading.

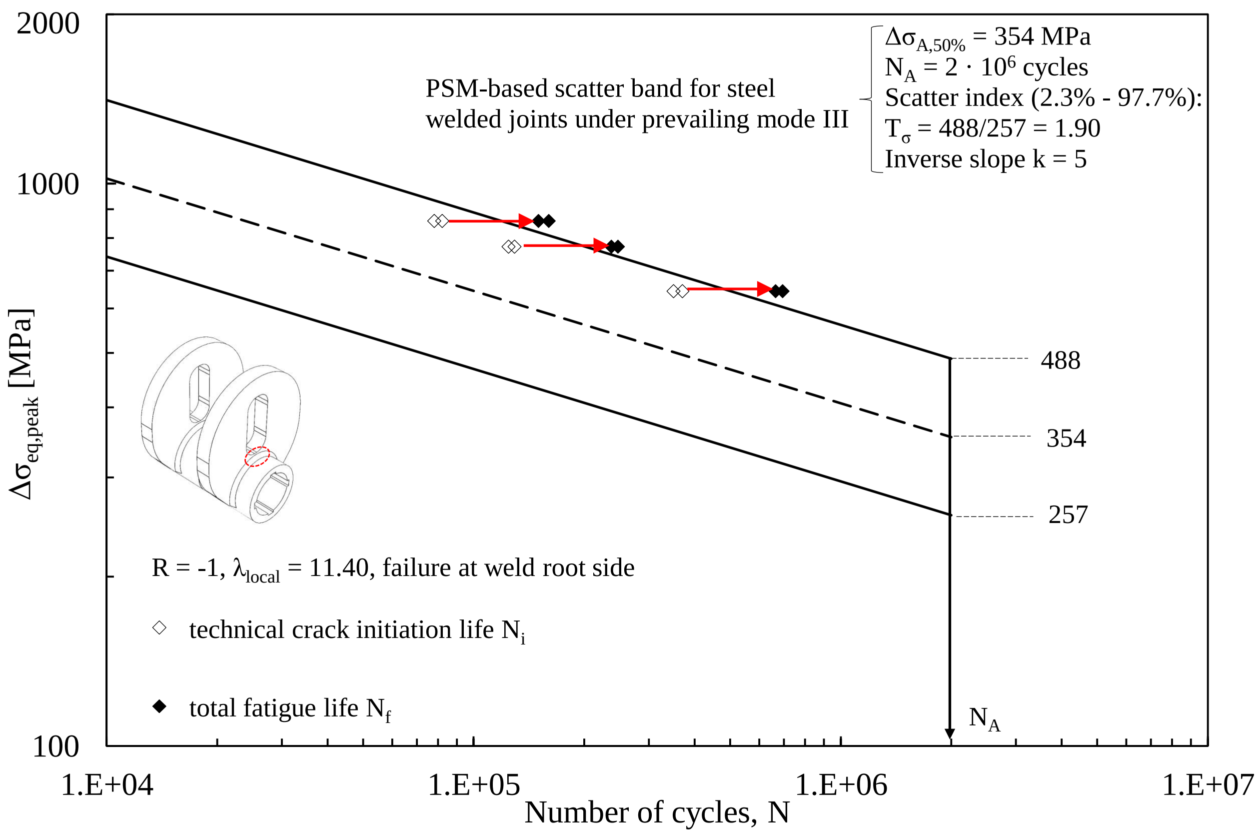

Figure 19: Fatigue assessment of root failures in fillet-welded structural steel joints (model 2 of Table 3) subject to in-phase multiaxial mode (I+III) stresses according to the PSM. The design scatter band was previously calibrated in Ref. [25] for pure torsion (mode III) loading.

Table 1: Values of constants and parameters f_{wi} in Eq. (12).

2α (deg)	λ_1 [(a)]	λ_2 [(a)]	λ_3 [(a)]	e_1 [(b)]	e_2 [(b)]	e_3 [(b)]	R_0 = 0.28 mm		
							f_{w1} [(c)]	f_{w2} [(d)]	f_{w3} [(e)]
0	0.500	0.500	0.500	0.133	0.340	0.414	1.410	5.522	3.478
135	0.674	-	0.800	0.118	-	0.259	1.064	-	1.877

(a): values from [13]
(b): values calculated with $\nu = 0.3$, e_1 and e_2 are referred to plane strain conditions
(c): values calculated with K^{*}_{FE} = 1.38 and d = 1 mm
(d): value calculated with K^{**}_{FE} = 3.38 and d = 1 mm
(e): values calculated with K^{***}_{FE} = 1.93 and d = 1 mm

Table 2. Conditions for applicability of Eqs. (8)-(10) by using ANSYS® FE code [22,24,25].

	Loading mode		
	Mode I	Mode II	Mode III
Eq.	(8)	(9)	(10)
K_{FE}	1.38 ± 3%	3.38± 3%	1.93± 3%
2D FE^	PLANE 42 or PLANE 182 (K-option 1 set to 3)		PLANE 25
3D FE^	SOLID 45 or SOLID 185 (K-option 2 set to 3)		
2α	$0° \le 2\alpha \le 135°$	$2\alpha = 0°$	$0° \le 2\alpha \le 135°$
Minimum a/d	3	14	3 (toe, $2\alpha \cong 135°$) 12 (root, $2\alpha = 0°$)
a – root side°	$a = \min\{l, z\}$	$a = \min\{l, z\}$	$a = \min\{l, z, t\}$
a – toe side°	$a = t$	-	$a = t$

^ finite elements of Ansys® Element Library
° *l*, *z*, *t* are defined in Fig. 3

Table 3: Joint geometries and FE analyses for fatigue strength assessment according to the PSM

Model	Joint Geometry – Loading Conditions	FE analyses
Model 1 tube-plate joint	see figures below	see figures below

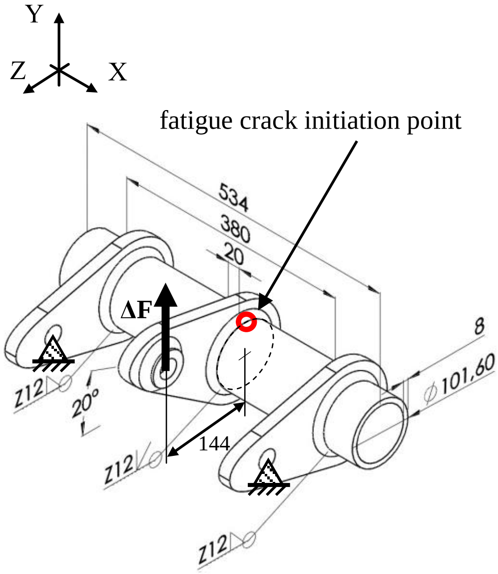

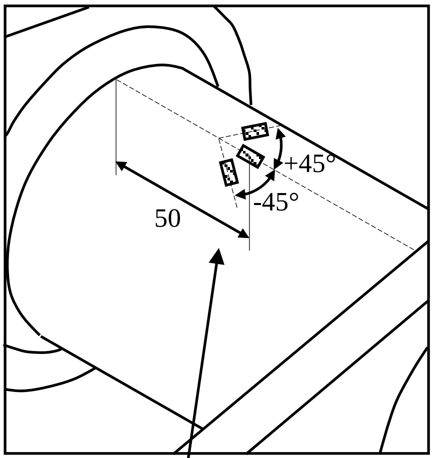

Location of a -45°/0°/+45° strain gauge rosette

PSM: sharp V-notch assumption at weld toe side

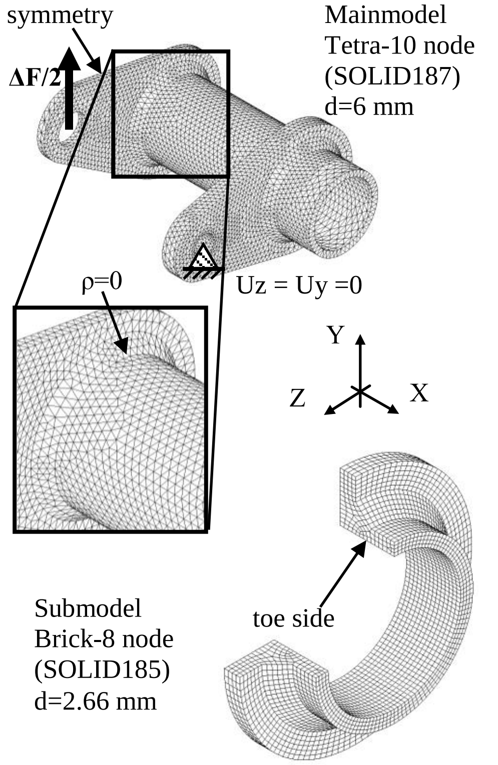

SED: radiused notch (ρ = 2 mm) at weld toe side

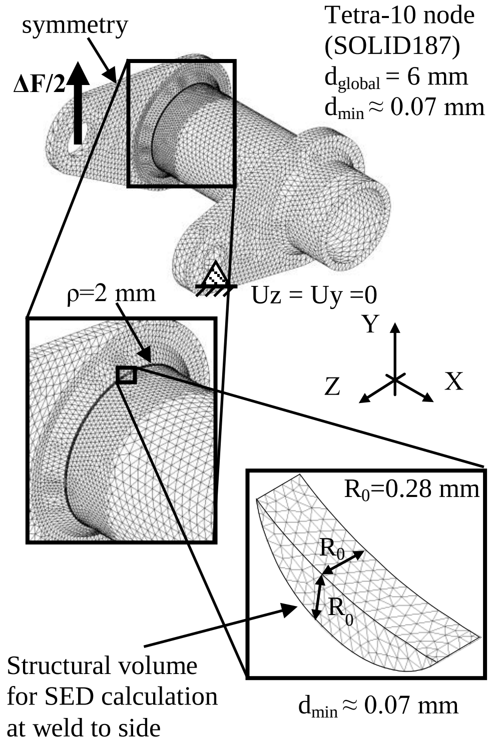

Model	Joint Geometry – Loading Conditions	FE analyses according to PSM
Model 2 scotch yoke joint		

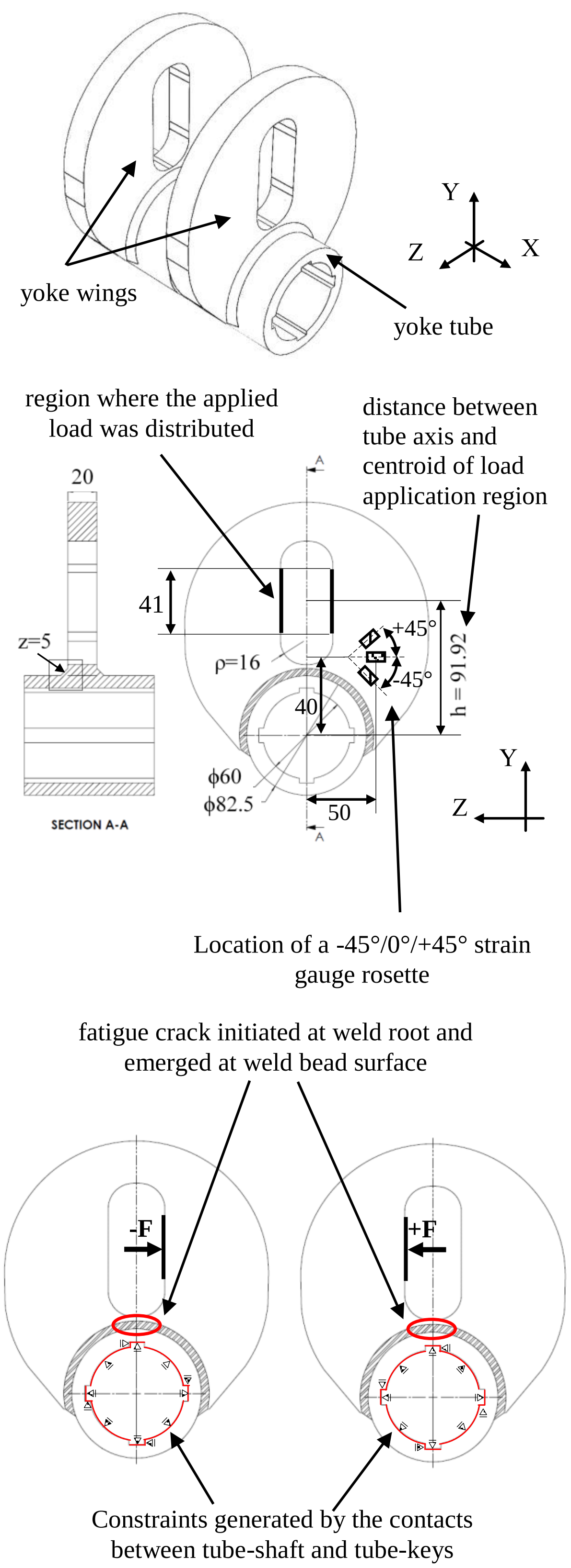

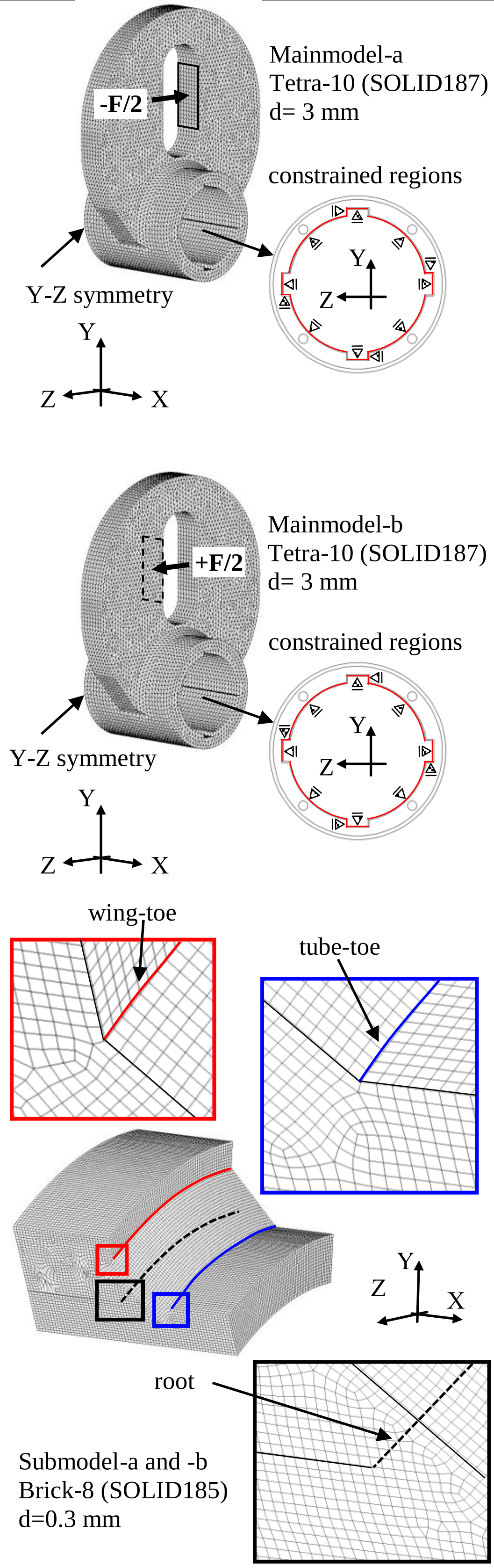

Table 4: Material and welding process of the welded joints.

Joint type	Model (Table 3)	Industrial application	Material	Yield strength [MPa]	Ultimate strength [MPa]	Welding process	Weld toe radius ρ [mm]
Full-penetration	(1)	Roundabout	S355JR	355	510	MIG	2
Fillet-welded	(2)	Scotch yoke for valve actuators	S355J2	355	510	MIG/MAG	-

Table 5: Testing conditions of the welded joints.

Joint type	Testing condition*	# tested specimens	Nominal load ratio R	Load range ΔF [kN]	Crack initiation/ failure criteria+	Crack initiation location	N_i/N_f	N_f cycles range
Full-penetration	AW SR°	7 7	0.1	100 ÷ 162	+0.1 mm/ +0.5 mm	weld toe	0.80÷0.96	$6 \cdot 10^4 \div 9 \cdot 10^5$
Fillet-welded	SR#	6	-1	150 ÷ 200	+0.1 mm/ +0.5 mm	weld root	0.50÷0.56	$1 \cdot 10^5 \div 7 \cdot 10^5$

* AW = as welded, SR = stress relieved

° post-welding heat treatment performed at 590°C for 2 h, heating and cooling being executed with a temperature gradient of 75°C/h.

\# post-welding heat treatment performed at 600°C for 1 h, heating and cooling being executed with a temperature gradient of 60°C/h.

\+ technical crack initiation and failure criteria defined for a given increase of the maximum displacement measured by the MTS controller.

Table 6: Residual stress measurement in full-penetration welded joints (model 1 of Table 3) by the X-ray diffraction method: adopted devices and experimental parameters.

Laboratory	University of Padova (UNIPD)	Fraunhofer IWM
X-ray device	Spider X	Stresstech G3
Specimen condition	2 AW, 1 SR	1 AW
Method	$sin^2\,\psi$ - method	
Measurement path	ϕ = 0° (see Fig. 5)	
Residual stress components	σ_{xx} and σ_{zz} (see Fig. 5)	
Acquisition time	500 s/ψ angle	-
$\psi -$ angles	5 ψ-angles 0° < ψ < 45°	σ_{xx}: 7 ψ-angles 0° < ψ < 45° σ_{zz}: 15 ψ-angles -45° < ψ < 45°